NASA TECHNICAL MEMORANDUM

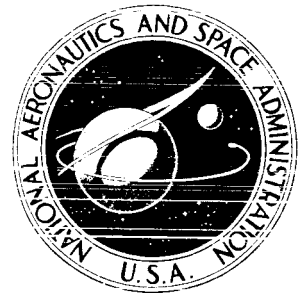

NASA TM X-2059

NASA TM X-2059

JET-PLUME-INDUCED FLOW SEPARATION ON AXISYMMETRIC BODIES AT MACH NUMBERS OF 3.00, 4.50, AND 6.00

by Robert J. McGhee

Langley Research Center
Hampton, Va. 23365

NATIONAL AERONAUTICS AND SPACE ADMINISTRATION • WASHINGTON, D. C. • AUGUST 1970

1. Report No.	2. Government Accession No.	3. Recipient's Catalog No.
NASA TM X-2059		

4. Title and Subtitle	5. Report Date
JET-PLUME-INDUCED FLOW SEPARATION ON AXISYMMETRIC BODIES AT MACH NUMBERS OF 3.00, 4.50, AND 6.00	August 1970
	6. Performing Organization Code
7. Author(s)	8. Performing Organization Report No.
Robert J. McGhee	L-7000
	10. Work Unit No.
9. Performing Organization Name and Address	126-13-10-22
NASA Langley Research Center Hampton, Va. 23365	11. Contract or Grant No.
	13. Type of Report and Period Covered
12. Sponsoring Agency Name and Address	Technical Memorandum
National Aeronautics and Space Administration Washington, D.C. 20546	14. Sponsoring Agency Code

15. Supplementary Notes

16. Abstract

Some effects of jet-plume-induced flow separation have been investigated at free-stream Mach numbers of 3.00, 4.50, and 6.00 on several axisymmetric bodies with various forebody and afterbody geometries. The investigation showed that increasing the jet-pressure ratio resulted in boundary-layer separation over large regions of the test models at free-stream Mach numbers of 4.50 and 6.00. Only small amounts of flow separation occurred at a free-stream Mach number of 3.00 for which the test jet-pressure ratios were considerably smaller than those for the higher Mach numbers. The separation angle measured at an angle of attack of 0° showed a primary dependency on jet-pressure ratio and was a weak function of model geometry. The separation length measured along the model surfaces was a function of both jet-pressure ratio and model geometry. Increasing the angle of attack resulted in decreases in both separation angle and separation length on the windward surface of the models. This result may be partially due to local Reynolds number changes, which cause changes in the type of separation. The local-surface-pressure coefficients in the separated-flow region compared reasonably well with the theoretical inviscid values for a cone at high jet-pressure ratios.

17. Key Words (Suggested by Author(s))	18. Distribution Statement
Plume-induced flow separation Boundary-layer separation Rocket exhaust Axisymmetric bodies	Unclassified – Unlimited

19. Security Classif. (of this report)	20. Security Classif. (of this page)	21. No. of Pages	22. Price*
Unclassified	Unclassified	37	$3.00

*For sale by the Clearinghouse for Federal Scientific and Technical Information
Springfield, Virginia 22151

JET-PLUME-INDUCED FLOW SEPARATION ON AXISYMMETRIC BODIES AT MACH NUMBERS OF 3.00, 4.50, AND 6.00

By Robert J. McGhee
Langley Research Center

SUMMARY

Some effects of jet-plume-induced flow separation have been investigated at free-stream Mach numbers of 3.00, 4.50, and 6.00 on several axisymmetric bodies with various forebody and afterbody geometries. Schlieren photographs were obtained for a wide range of jet-pressure ratios (ratios of jet-exit static pressure to free-stream static pressure) for an angle-of-attack range from about 0° to 13°. In addition, surface-pressure data for one configuration with a conical forebody and a cylindrical afterbody were measured in the separated-flow region for an angle-of-attack range from about -6° to 8°. Most of the present tests were conducted at free-stream Reynolds numbers per meter of 6.90×10^6 and 3.60×10^6 for free-stream Mach numbers of 3.00 and 6.00, respectively.

The investigation showed that increasing the jet-pressure ratio resulted in boundary-layer separation over large regions of the test models at free-stream Mach numbers of 4.50 and 6.00. Only small amounts of flow separation occurred at a free-stream Mach number of 3.00 for which the test jet-pressure ratios were considerably smaller than those for the higher Mach numbers. The separation angle measured at an angle of attack of 0° showed a primary dependency on jet-pressure ratio and was a weak function of model geometry. The separation length measured along the model surfaces was a function of both jet-pressure ratio and model geometry. Increasing the angle of attack resulted in decreases in both separation angle and separation length on the windward surface of the models. This result may be partially due to local Reynolds number changes, which cause changes in the type of separation. The local-surface-pressure coefficients in the separated-flow region compared reasonably well with the theoretical inviscid values for a cone at high jet-pressure ratios.

INTRODUCTION

Flight at high altitudes and high Mach numbers often causes rocket-motor nozzles to exhaust at static pressures much greater than the ambient pressure. For even

moderate underexpansion, large billowing exhaust plumes result and may promote boundary-layer separation as well as high surface heating and large local loads from flow impingement upon adjacent surfaces. If ionized exhaust gases are involved, the plumes may attenuate radio waves. Some investigations of these problem areas have been conducted and the results are reported in references 1 to 4. Reference 1 shows that jet-plume-induced flow separation has a significant effect on the aerodynamic forces and moments of axisymmetric bodies. Significant decreases in normal-force-curve slopes and static stability are shown for a free-stream Mach number of 6.00.

In an attempt to obtain improved knowledge of jet-plume-induced separation phenomena, the present investigation has been conducted on several axisymmetric bodies with various forebody and afterbody geometries. Schlieren photographs were obtained for a wide range of jet-pressure ratios and several Mach numbers. In addition, one configuration with a conical forebody and a cylindrical afterbody was instrumented with four surface-pressure orifices to measure the separation-induced pressures on the model caused by the underexpanded exhaust-nozzle flow. A supersonic exhaust nozzle was used with compressed gaseous nitrogen to obtain the jet plume.

The investigation was conducted in a 2-foot hypersonic facility at the Langley Research Center. For most of the present tests, the Reynolds numbers per meter were approximately 6.90×10^6 and 3.60×10^6 at free-stream Mach numbers of 3.00 and 6.00, respectively. The angle of attack was varied from about -6° to 13°.

SYMBOLS

C_p pressure coefficient, $\frac{2}{\gamma M_\infty^2}\left(\frac{p}{p_\infty} - 1\right)$

d diameter of centerbody, 3.04 centimeters

l_s separation length based on schlieren measurements, distance from separation point to model base

L total model length

M Mach number

p static pressure

q dynamic pressure

R	Reynolds number per meter
x	longitudinal coordinate
y	lateral coordinate
x/d	orifice location in body diameters (see fig. 4)
α	angle of attack
γ	ratio of specific heats
θ_s	separation angle based on schlieren measurements (see fig. 6)

Subscripts:

j	jet-exit condition, calculated from ideal one-dimensional nozzle flow
o	condition at beginning of interaction
r	condition at reattachment
∞	free-stream condition

APPARATUS AND TESTS

Models

The general arrangement of a typical model is shown in figure 1, which illustrates the sting and nozzle assembly. Each configuration consisted of a cylindrical centerbody to which were attached a forebody and an afterbody. Details of the model components and the supersonic nozzle are shown in figures 2 and 3, respectively, and configuration designations are identified in table I.

The forebodies consisted of an ogive with a nose radius of 0.10 cm, a 30° half-angle cone, and a 15° half-angle cone. The afterbodies consisted of a 20° flare, a straight cylinder, and a cylindrical body with four fins having 30° sweptback leading edges. (See fig. 2.) The cylindrical centerbody had a length-diameter ratio of 2.83.

The model support sting, a hollow steel tube, allowed the gaseous nitrogen from the supply tank to be emptied through louvers into the settling chamber of the nozzle. The

supersonic nozzle was designed as an annular nozzle because only the outer plume boundary was simulated. Allowance was made in the nozzle design for the presence of the center support sting. The nozzle had an area ratio (ratio of exit area to throat area) of 2.07, a calculated exit Mach number of 2.24, and a divergence angle ($17^{o}57'$) which approximated that for a representative rocket engine. Cold gaseous nitrogen at approximately local atmospheric temperature was used to obtain the exhaust plume.

Wind Tunnel

The tests were conducted in a 2-foot hypersonic facility at the Langley Research Center. This wind tunnel, described in reference 5, is an ejector-type facility which provides continuous flow at high Mach numbers and low densities. The average test conditions for the present investigation are shown in the following table:

M_∞	Stagnation temperature, ^{o}K	Stagnation pressure, kN/m^2	Static pressure, kN/m^2	Reynolds number per meter
3.00	311	100	2.31	6.90×10^6
4.50	422	144	.57	3.08
6.00	422	319	.20	3.60

Nitrogen Supply

High-pressure gaseous nitrogen was generated by pumping liquid nitrogen to the required storage pressure and converting it from liquid to gas in a steam-actuated heat exchanger. The high-pressure gaseous nitrogen was then stored in a tank farm with a capacity of 22.65 m^3. Suitable pressure-reducing and pressure-regulating valves were remotely controlled to obtain the nitrogen gas pressure in a manifold outside the test section which, in turn, fed the nozzle plenum chamber in the model. Once the correct pressure was obtained in the manifold, a quick-acting guillotine valve was employed to initiate and terminate the flow to the nozzle.

Instrumentation

Four static-pressure orifices (0.15 cm in diameter) were located on the cylindrical centerbody of configuration 1 in the plane of symmetry as shown in figure 4. Simultaneous measurements of pressures at the four orifices, as well as the nozzle plenum pressure, were obtained from absolute-pressure-measuring transducers. Data were obtained by a high-speed data-acquisition system and recorded on magnetic tape. Schlieren photographs were taken with the use of a 2-μsec flash from a xenon light source in order to make a visual study of the jet-plume-induced separation phenomenon.

Tests and Accuracy

Schlieren photographs were obtained at free-stream Mach numbers of 3.00, 4.50, and 6.00 for an angle-of-attack range from about 0° to 13°. Local-surface-pressure data (p/p_{∞}) were obtained for configuration 1 at Mach numbers of 3.00 and 6.00 for an angle-of-attack range from about -6° to 8°. The jet-pressure ratio p_j/p_{∞} varied from jet off to about 330 at $M_{\infty} = 3.00$ and from jet off to about 4700 at $M_{\infty} = 6.00$. All data were obtained with the model smooth; that is, no boundary-layer transition strips were used. At the Reynolds numbers of these tests, laminar flow was considered to exist over the entire model at jet-off conditions.

The ratios p_j/p_{∞} and p/p_{∞} quoted herein are estimated to be accurate within ±2 percent. The Mach number in the region of the test models was accurate within ±0.04. Angle-of-attack values are estimated to be accurate within $\pm 0.1^{\circ}$.

RESULTS AND DISCUSSION

The results of this investigation have been arranged to illustrate the jet-plume-induced flow field which results from underexpanded rocket-motor nozzles operating at free-stream Mach numbers of 3.00, 4.50, and 6.00. Figures 5 and 6 illustrate separation characteristics for an axisymmetric flow field. Schlieren photographs of the flow fields with and without jet pluming for the configurations of the present investigation are given in figures 7 to 11, and the local-surface-pressure data for configuration 1 are presented in figure 12. Figures 13 to 15 show the effect of an increase in jet-pressure ratio (an increase in the size of the jet plume) on separation angle and length. Figure 16 compares the pressure coefficients for configuration 1 with the inviscid values for a wedge and cone.

Boundary-Layer Separation Characteristics

The analysis of reference 6 has shown that for a two-dimensional laminar boundary-layer separation, the pressure in the separated region is a function of M_0, M_r, and Reynolds number (that is, whether the flow between separation and reattachment is laminar, transitional, or turbulent). For the present investigation, changes in model forebody and afterbody geometry as well as the presence of a large jet plume would apparently affect the flow conditions. Sketches and schlieren photographs of the flow fields for a cone-cylinder configuration with separation induced by a jet plume are shown in figure 6. Figure 5 compares the boundary-layer separation characteristics for a cone-cylinder-flare configuration with those for a cone-cylinder configuration with a plume.

Effect of Jet-Pressure Ratio and Angle of Attack

Surface pressures.- The local surface pressures measured for configuration 1 at $M_\infty = 3.00$ and 6.00 are presented in figure 12 in terms of p/p_∞ as a function of jet-pressure ratio p_j/p_∞ and angle of attack α. At $M_\infty = 3.00$ the local surface pressures were essentially independent of p_j/p_∞ and therefore indicates essentially no flow separation at the location of the pressure orifices (see fig. 12(a)), although the schlieren photographs indicate some separation for the higher values of p_j/p_∞. At $M_\infty = 6.00$ greater values of p_j/p_∞ were obtainable than at $M_\infty = 3.00$, and the local surface pressures increased as p_j/p_∞ was increased (see figs. 12(b) and 12(c)). This increase in surface pressures resulted from an increase in the extent of separation as the size of the jet plume increased. The larger jet plumes may change the conditions at reattachment and the type of separation; the flow may become transitional at the higher values of p_j/p_∞. Increasing the model angle of attack in the presence of large jet plumes resulted in a decrease in the extent of flow separation on the windward side of the models and an increase on the leeward side. However, increasing the angle of attack also changes the local Reynolds number, and thus the decrease in the extent of flow separation on the windward side of the model could result partially from changes in the type of separation.

Separation angle.- The separation angle θ_s is shown in figure 13 as a function of p_j/q_∞ and p_j/p_∞ for the test configurations at $\alpha = 0^\circ$ and $M_\infty = 4.50$ and 6.00. In figure 14, θ_s is shown as a function of p_j/p_∞ for the test configurations at $\alpha = 4^\circ$ and 8° and $M_\infty = 4.50$ and 6.00. Values of θ_s were measured from the schlieren photographs as shown in figure 6. At zero angle of attack (fig. 13), the separation angle was affected only slightly by model geometry and showed a primary dependency on jet-pressure ratio. Values of θ_s increased to a maximum of approximately 13° at $p_j/p_\infty = 4500$. Increases in angle of attack (see fig. 14) decreased θ_s on the windward surface and increased θ_s on the leeward surface as p_j/p_∞ was increased.

Separation length.- Although θ_s was affected only slightly by model geometry for $\alpha = 0^\circ$, separation length l_s was dependent on model geometry. The separation length was measured along the model surface from the model base to the point where the shock from the separated region intersected the body. The data of figure 15 for $M_\infty = 4.50$ and 6.00 show that as p_j/p_∞ was increased, the separation length along the body surfaces increase and approach the shoulder (forebody-centerbody juncture) for each conical-forebody configuration. The shoulders for configurations 1, 4, and 5 are located at $l_s/L = 0.70$, and the shoulder for configuration 2 is at $l_s/L = 0.84$. The ogive-forebody—cylinder junction of configuration 3 is located at $l_s/L = 0.65$. The favorable effect of angle of attack in decreasing l_s on the windward side of the models for $M_\infty = 4.50$ and 6.00 is also indicated. As previously mentioned, the extent of flow separation depends on whether the separation is laminar or transitional. Changes in

either model geometry or angle of attack, as well as the presence of the large jet plumes, could affect the type of separation. The various afterbodies of this investigation had small effects on l_s as p_j/p_∞ was increased because of the predominate effects of the large jet plumes on the flow field.

Surface-Pressure Coefficient

Figure 16 presents the pressure coefficient C_p for configuration 1 at $M_\infty = 6.00$ and $\alpha = 0^\circ$ as a function of flow-deflection angle. Separation angles measured from the schlieren photographs were used as the flow-deflection angles for the experimental data. Theoretical values of the inviscid pressure coefficients for a wedge and a cone were calculated by using reference 7 and are presented for comparison. A correction of 1.5° has been applied to all experimental values of θ_s to account for the boundary-layer growth rate at jet-off conditions (measured from fig. 7(b)) and to make the values of C_p comparable with the inviscid values from reference 7. At the smaller flow-deflection angles, corresponding to low values of p_j/p_∞, the experimental data fall below the theoretical inviscid values for a cone; however, at the larger flow-deflection angles, corresponding to high values of p_j/p_∞, the experimental values of C_p correlate with the theoretical cone values.

CONCLUDING REMARKS

Some effects of jet-plume-induced flow separation have been investigated at free-stream Mach numbers of 3.00, 4.50, and 6.00 on several axisymmetric bodies with various forebody and afterbody geometries. Schlieren photographs were obtained for a wide range of jet-pressure ratios (ratios of jet-exit static pressure to free-stream static pressure) for an angle-of-attack range from about 0° to 13°. In addition, surface-pressure data for one configuration with a conical forebody and a cylindrical afterbody were measured in the separated-flow region for an angle-of-attack range from about -6° to 8°. Most of the present tests were conducted at free-stream Reynolds numbers per meter of 6.90×10^6 and 3.60×10^6 for free-stream Mach numbers of 3.00 and 6.00, respectively.

As the size of the jet plume was increased by increasing the jet-pressure ratio, boundary-layer separation occurred over large regions of the test models at free-stream Mach numbers of 4.50 and 6.00. Only small amounts of flow separation occurred at a free-stream Mach number of 3.00 for which the test jet-pressure ratios were considerably smaller than those for the higher Mach numbers. The separation angle measured at an angle of attack of 0° showed a primary dependency on jet-pressure ratio and was a weak function of model geometry. The separation length measured along the model

surfaces was a function of both jet-pressure ratio and model geometry. Increases in angle of attack in the presence of jet pluming resulted in decreases in both separation angle and separation length on the windward surface of the models. This result may be partially due to local Reynolds number changes, which cause changes in the type of separation. The local-surface-pressure coefficients in the separated-flow region compared reasonably well with the theoretical inviscid values for a cone at high jet-pressure ratios.

Langley Research Center,
National Aeronautics and Space Administration,
Hampton, Va., May 5, 1970.

REFERENCES

1. McGhee, Robert J.: Some Effects of Jet Pluming on the Static Stability of Ballistic Bodies at a Mach Number of 6.00. NASA TN D-3698, 1966.

2. Hinson, William F.; and McGhee, Robert J.: Effects of Jet Pluming on the Static Stability of Five Rocket Models at Mach Numbers of 4, 5, and 6 and Static Pressure Ratios up to 26 000. NASA TN D-4064, 1967.

3. McGhee, Robert J.; and Martin, James A.: Exploratory Investigation of Flow Field Resulting From Forward-Facing Nozzles Exhausting Near a Large Cylindrical Body at Free-Stream Mach Numbers of 3.0 and 6.0. NASA TN D-5030, 1969.

4. Saturn V Engineering: Saturn V Exhaust Effects on Radio Systems Performance. Doc. No. D5-15606 (Contract NAS8-5608), Boeing Co., Oct. 3, 1966.

5. Stokes, George M.: Description of a 2-Foot Hypersonic Facility at the Langley Research Center. NASA TN D-939, 1961.

6. Chapman, Dean R.; Kuehn, Donald M.; and Larson, Howard K.: Investigation of Separated Flows in Supersonic and Subsonic Streams With Emphasis on the Effect of Transition. NACA Rep. 1356, 1958.

7. Ames Research Staff: Equations, Tables, and Charts for Compressible Flow. NACA Rep. 1135, 1953. (Supersedes NACA TN 1428.)

TABLE I.- CONFIGURATION IDENTIFICATION

Figure	Configuration	Forebody	Afterbody
7, 12, 13, 14, 15, 16	1	15^{o} half-angle cone	Cylinder
8, 13, 14, 15	2	30^{o} half-angle cone	Cylinder
9, 13, 14, 15	3	Ogive	Cylinder
10, 13, 14, 15	4	15^{o} half-angle cone	Flare
11, 13, 14, 15	5	15^{o} half-angle cone	Fin

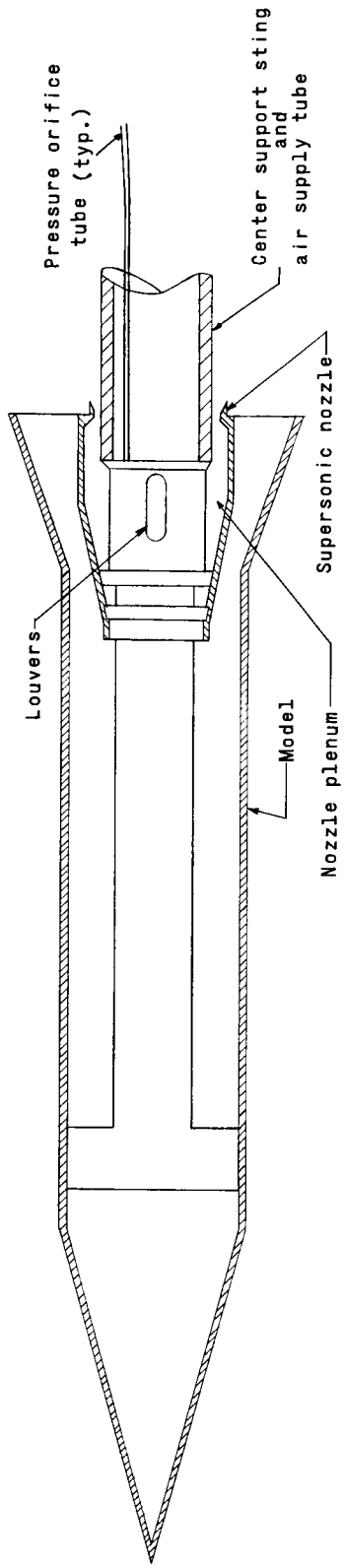

Figure 1.- Sketch of configuration 4 showing sting and nozzle arrangement.

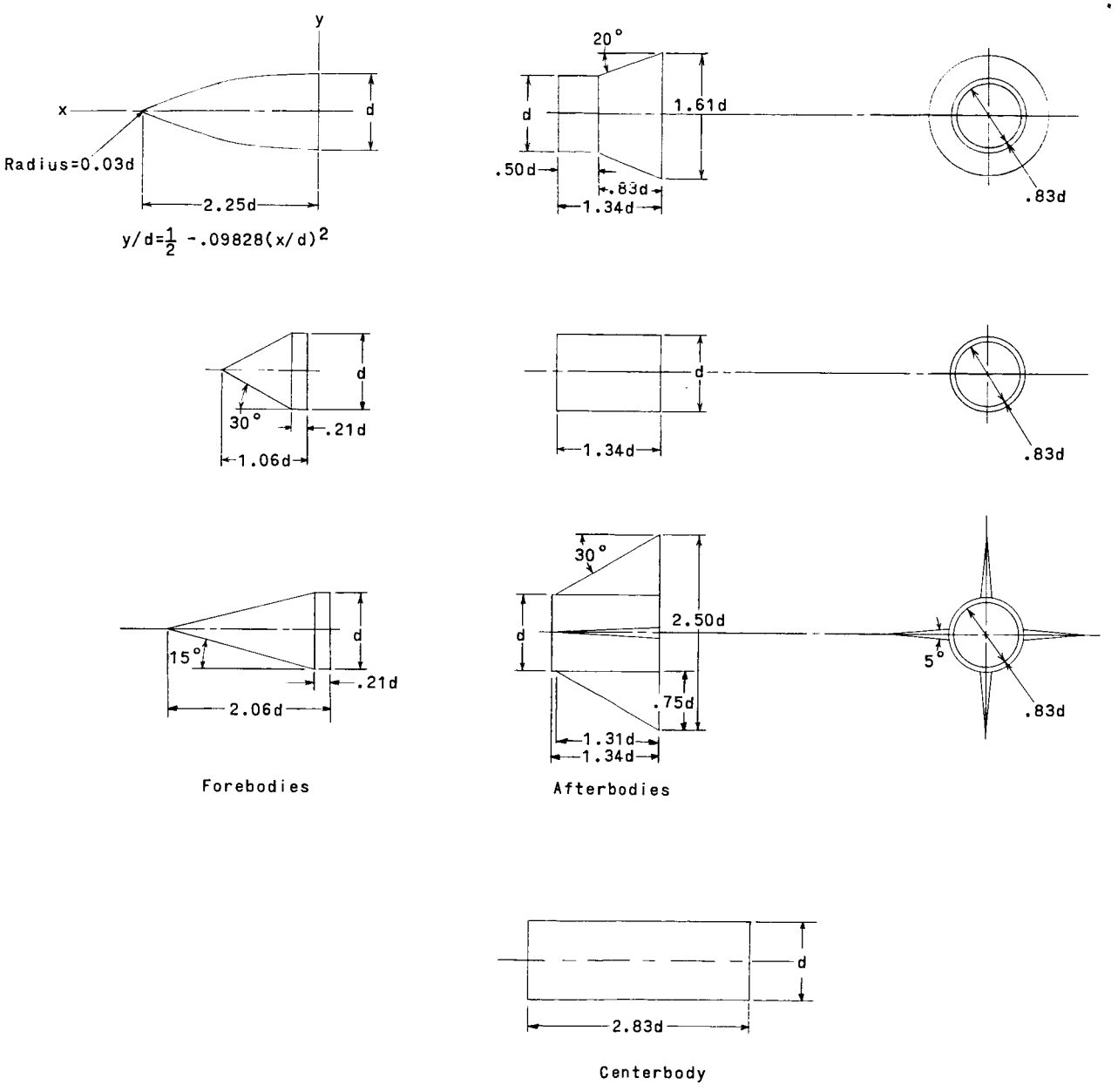

Figure 2.- Details of models tested. d = 3.04 cm.

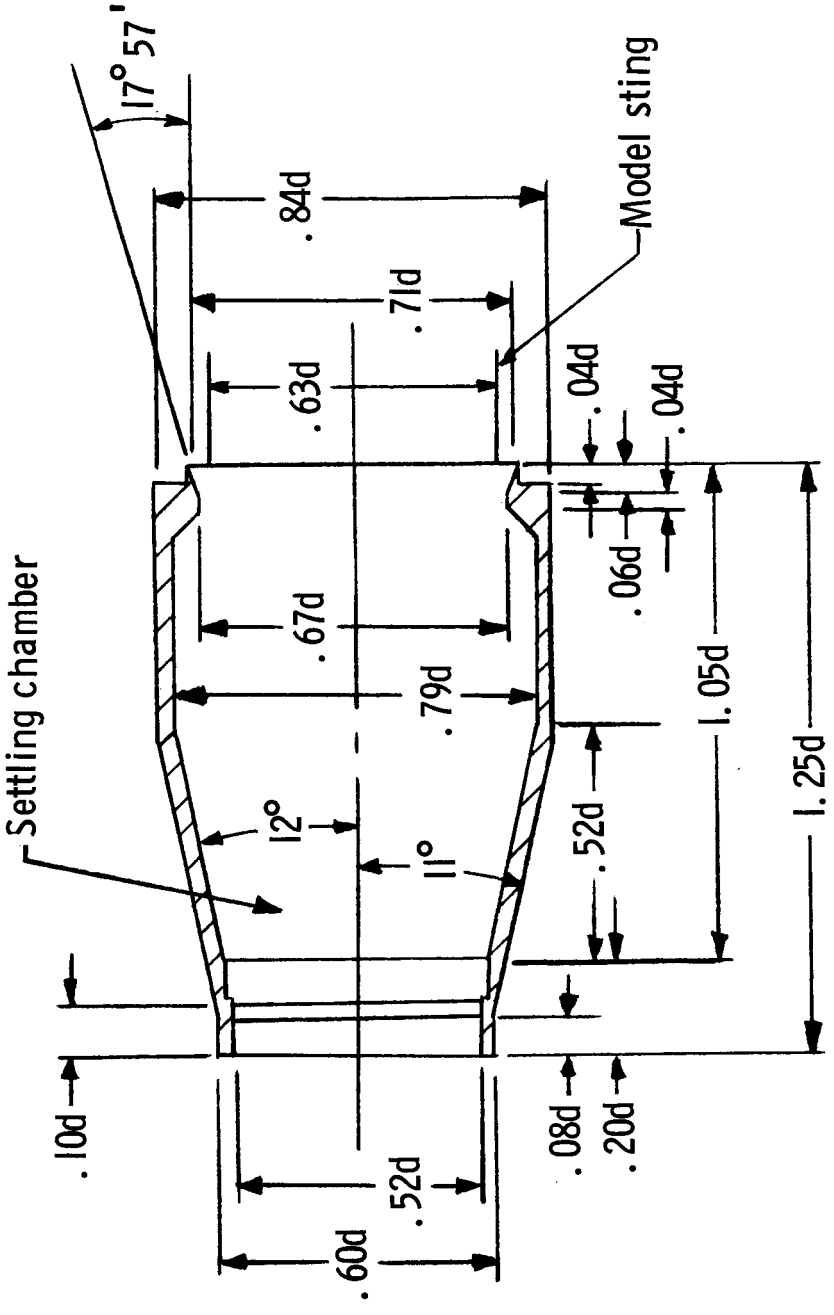

Figure 3.- Details of supersonic nozzle. d = 3.04 cm.

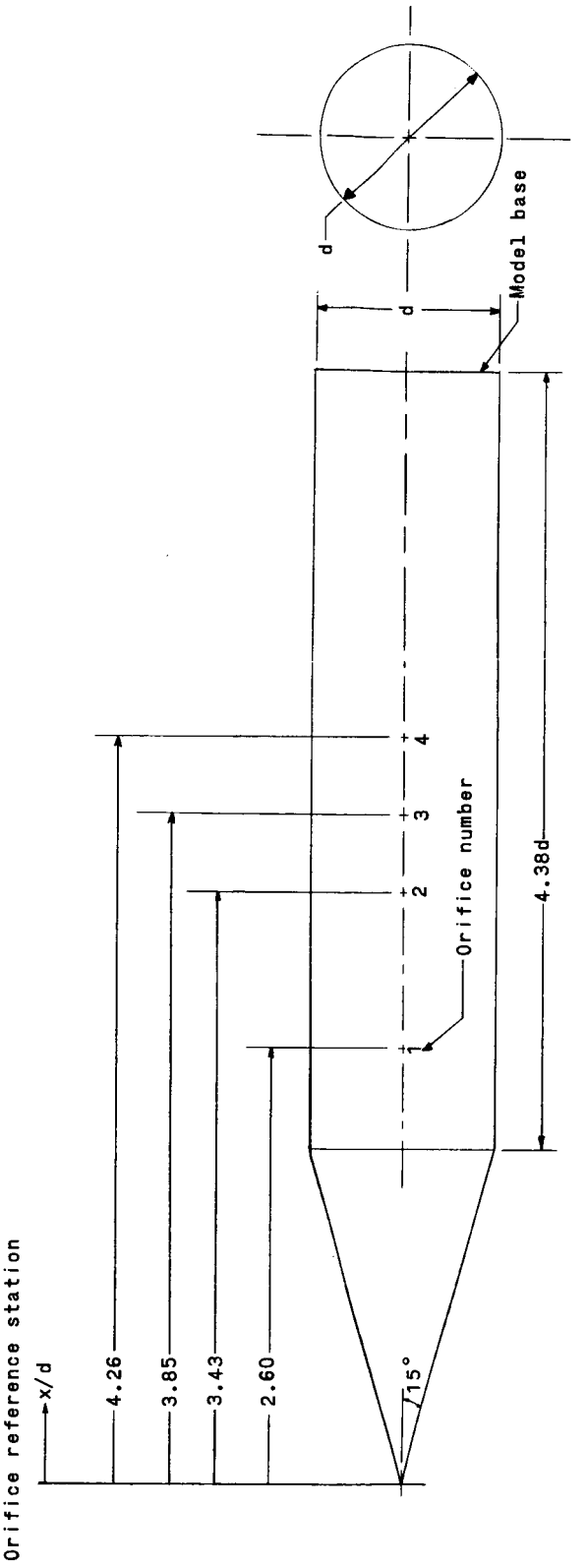

Figure 4.- Orifice locations for configuration 1. d = 3.04 cm.

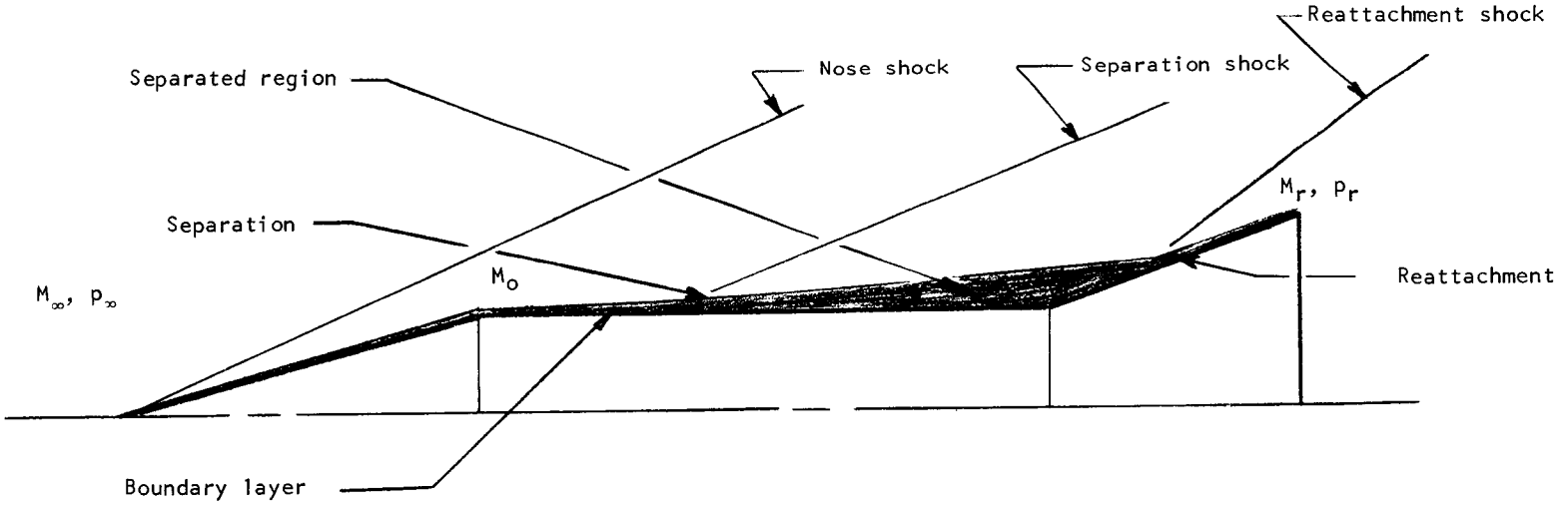

(a) Cone-cylinder-flare configuration.

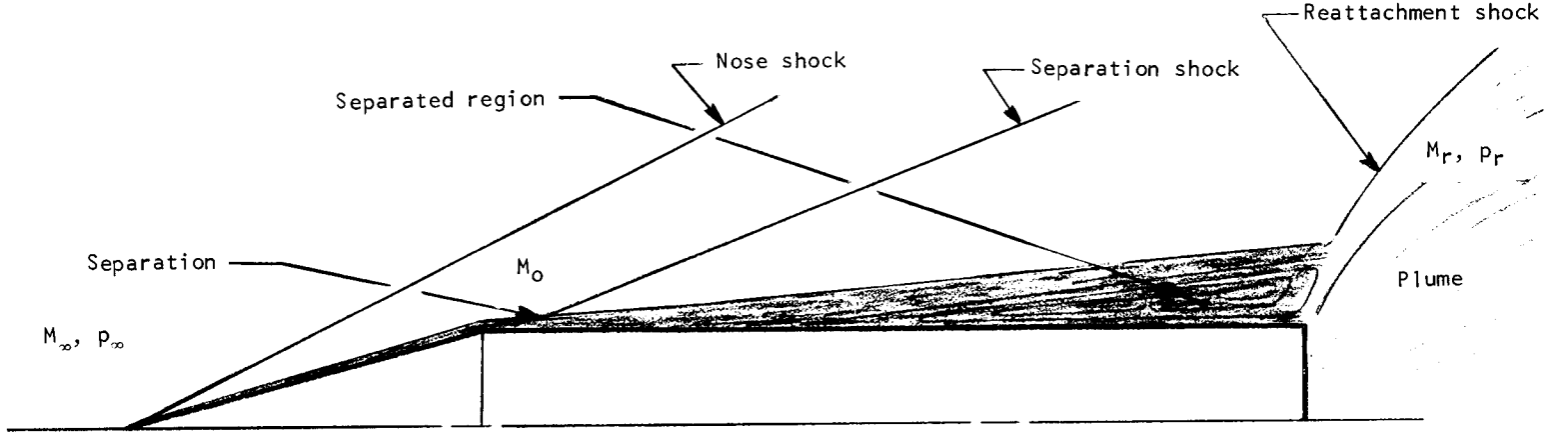

(b) Cone-cylinder configuration with plume.

Figure 5.- Boundary-layer separation characteristics.

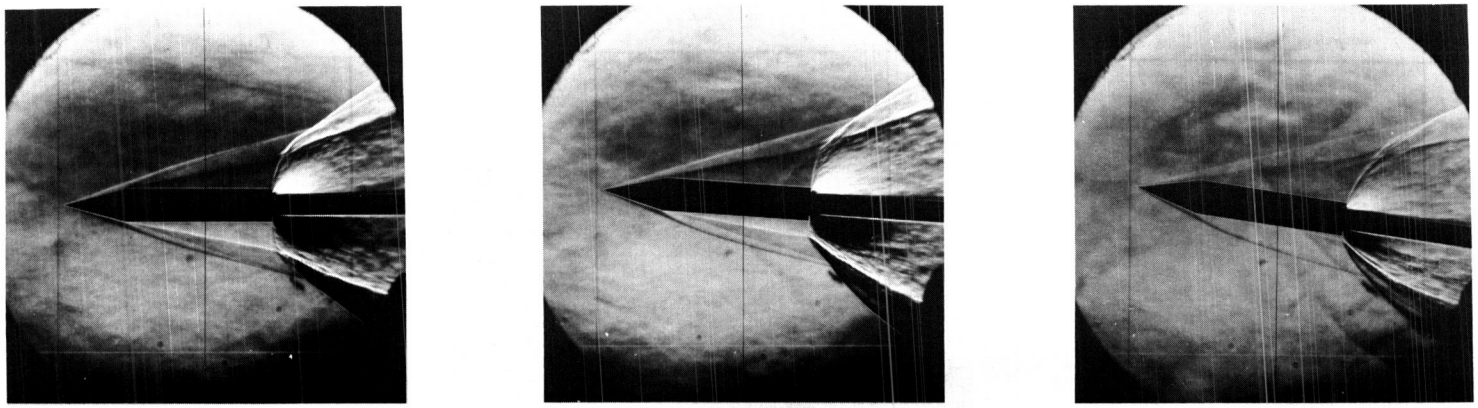

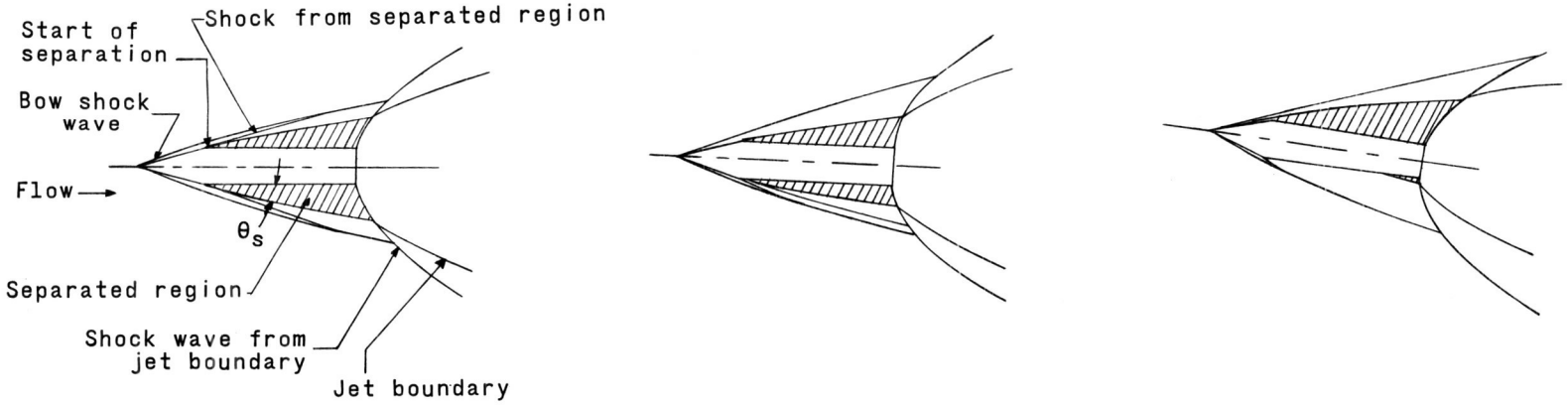

Figure 6.- Schematic representation of the flow-field nomenclature.

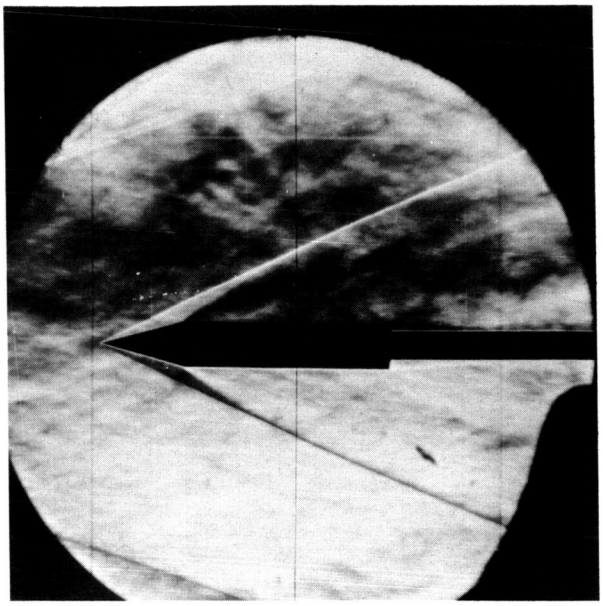

Jet off

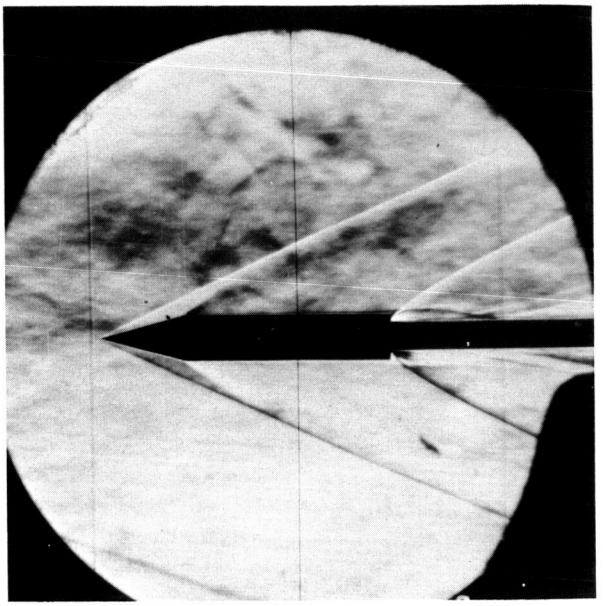

p_j/p_∞=27

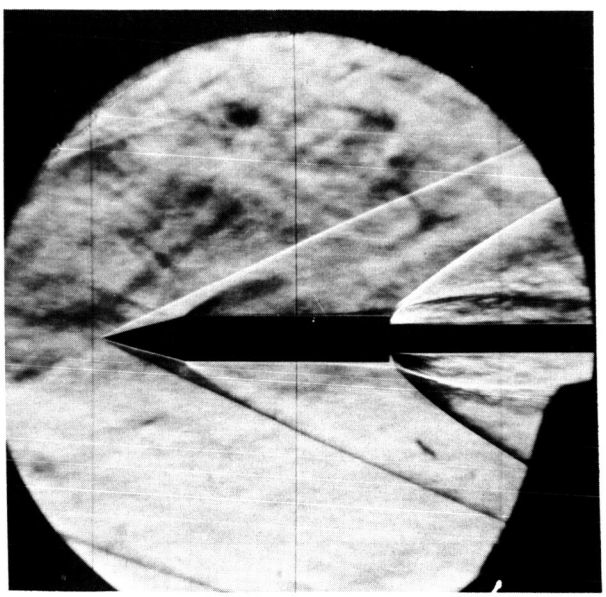

p_j/p_∞=95

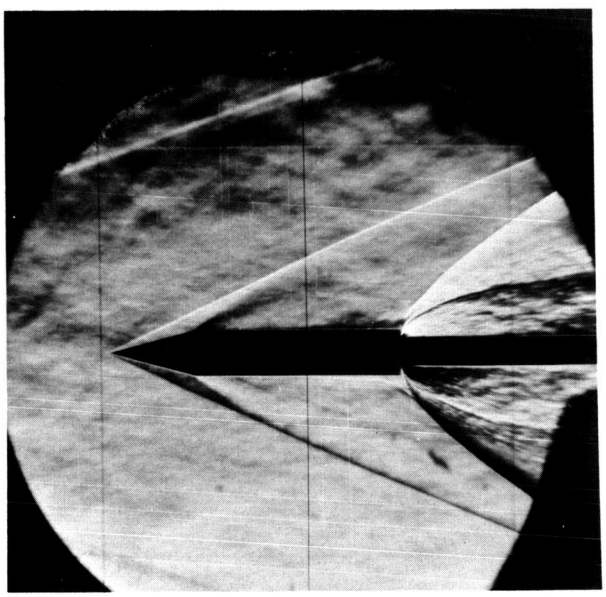

p_j/p_∞=244

(a) $M_\infty = 3.00$; $\alpha = 0^0$. L-70-1644

Figure 7.- Schlieren photographs for configuration 1.

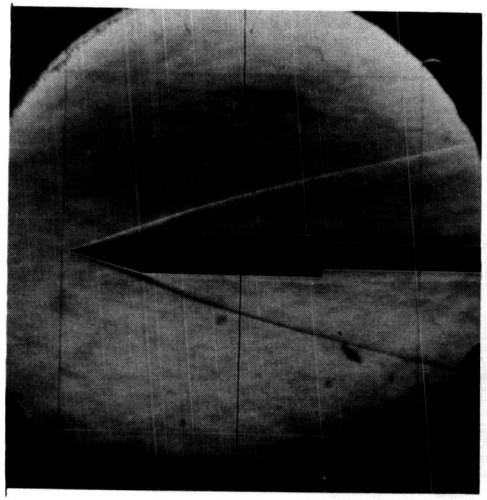

Jet off

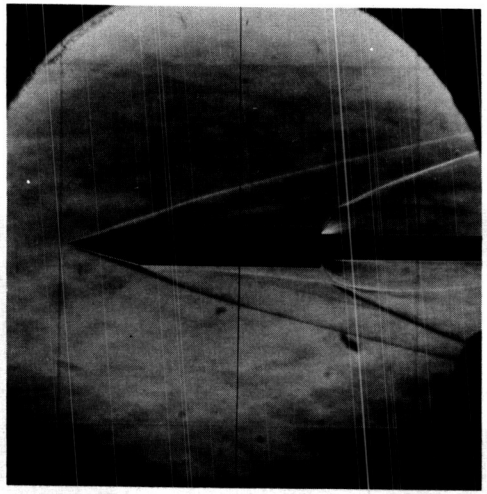

p_j/p_∞=157

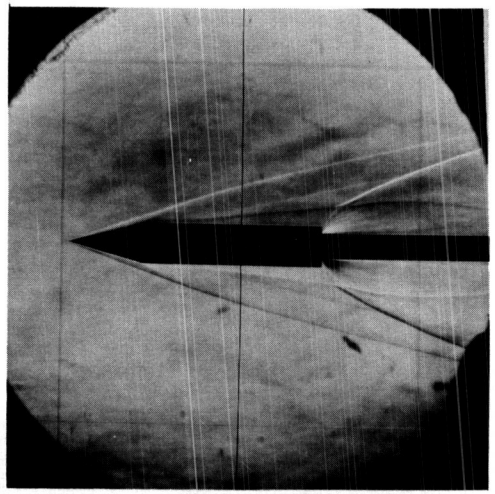

p_j/p_∞=223

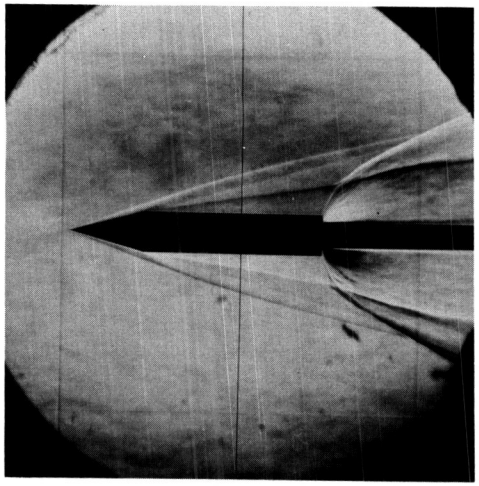

p_j/p_∞=908

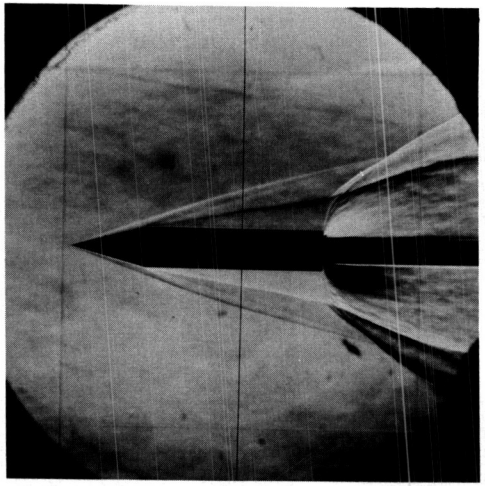

p_j/p_∞=1824

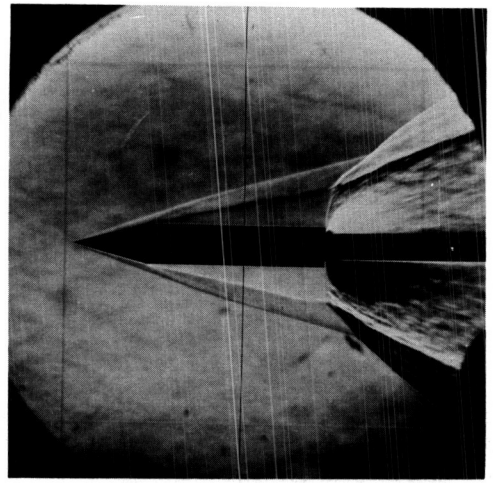

p_j/p_∞=3710

(b) $M_\infty = 6.00$; $\alpha = 0^0$.

L-70-1645

Figure 7.- Continued.

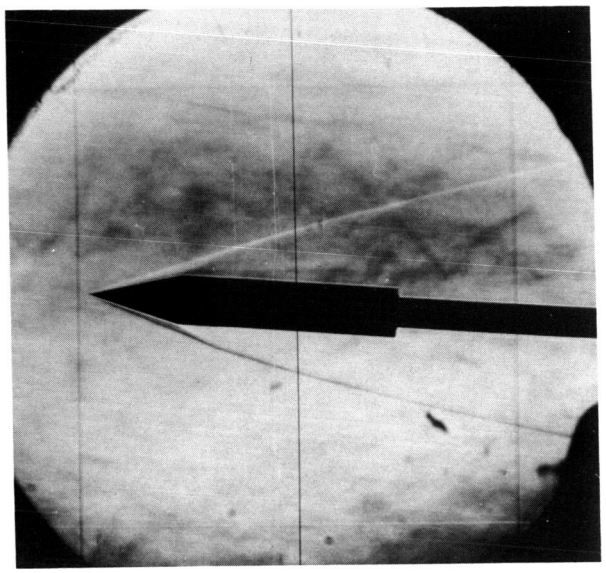

Jet off

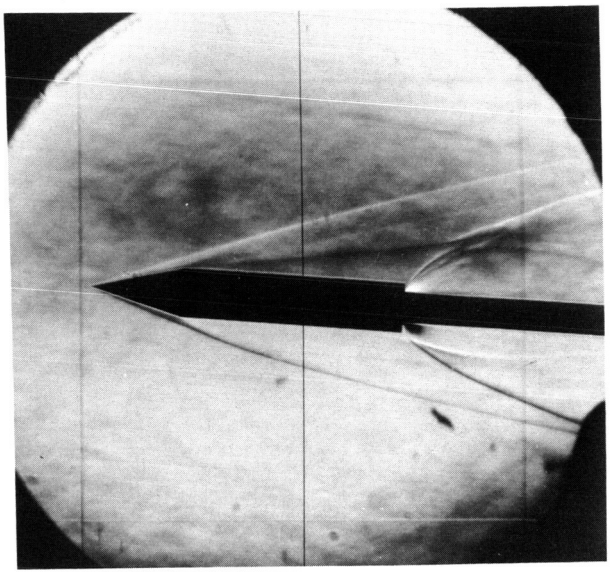

p_j/p_∞=153

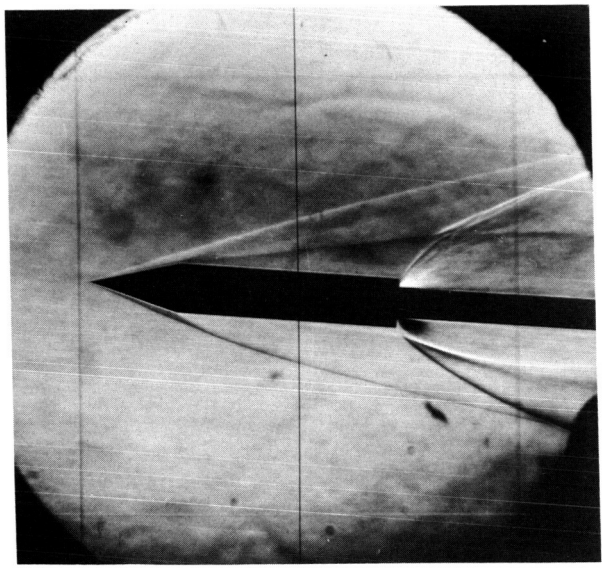

p_j/p_∞=299

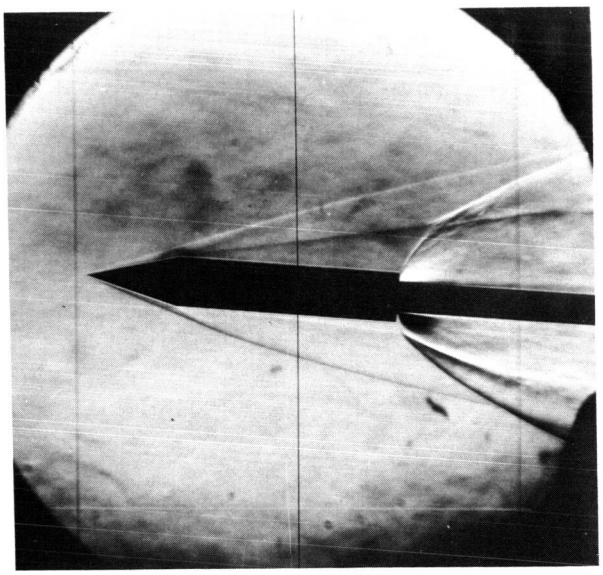

p_j/p_∞=603

(c) $M_\infty = 6.00$; $\alpha = 4^0$. L-70-1646

Figure 7.- Continued.

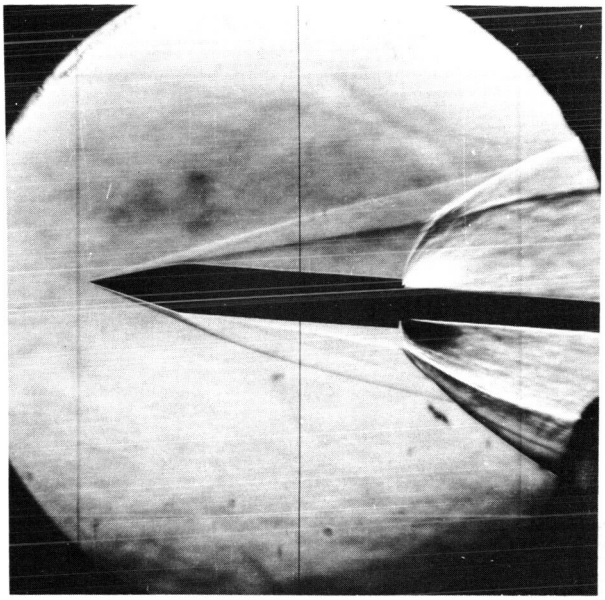

$p_j/p_\infty=1521$

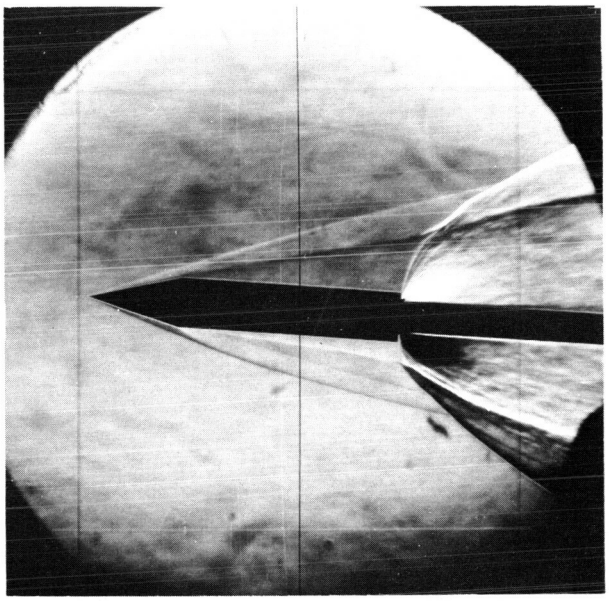

$p_j/p_\infty=1829$

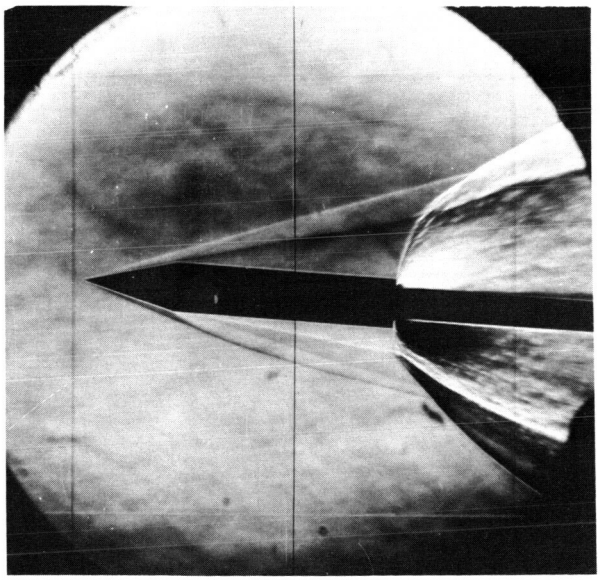

$p_j/p_\infty=2736$

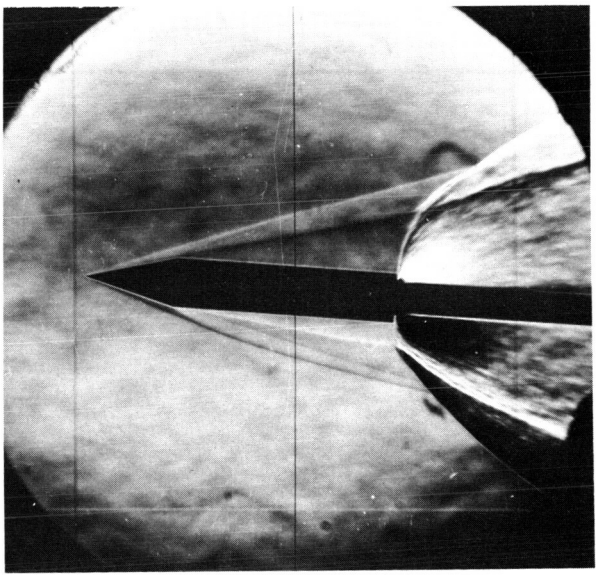

$p_j/p_\infty=3019$

(c) Concluded.

L-70-1647

Figure 7.- Concluded.

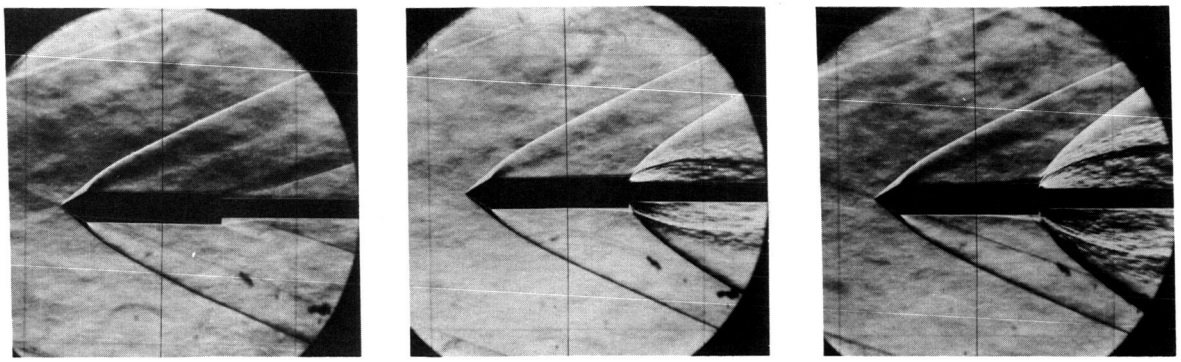

Jet off | p_j/p_∞=117 | p_j/p_∞=272

(a) M_∞ = 3.00.

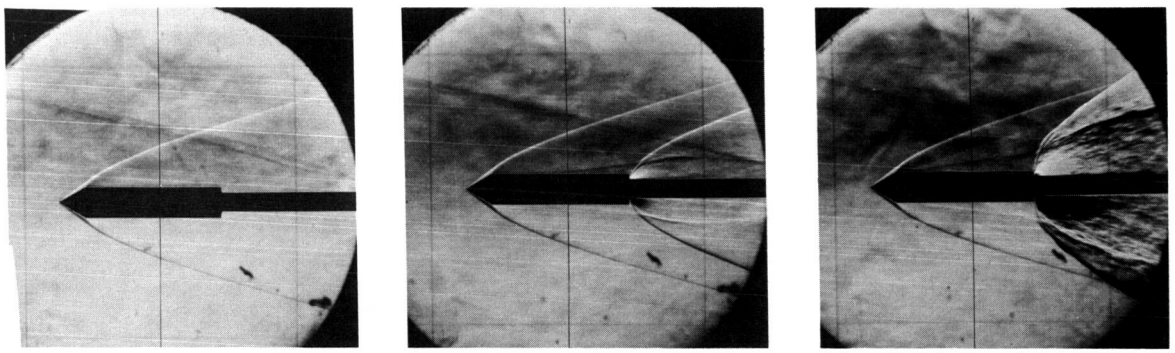

Jet off | p_j/p_∞=140 | p_j/p_∞=1278

(b) M_∞ = 4.50.

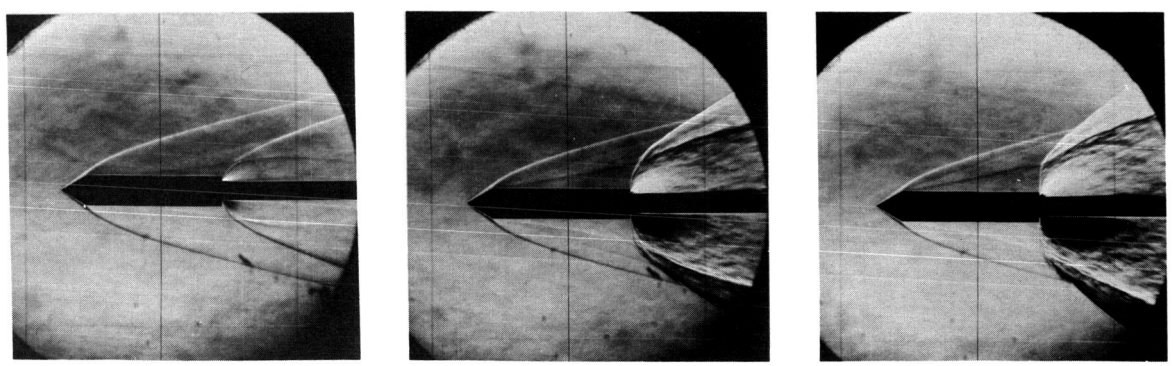

p_j/p_∞=193 | p_j/p_∞=2121 | p_j/p_∞=4472

(c) M_∞ = 6.00.

Figure 8.- Schlieren photographs for configuration 2. $\alpha = 0^0$. L-70-1648

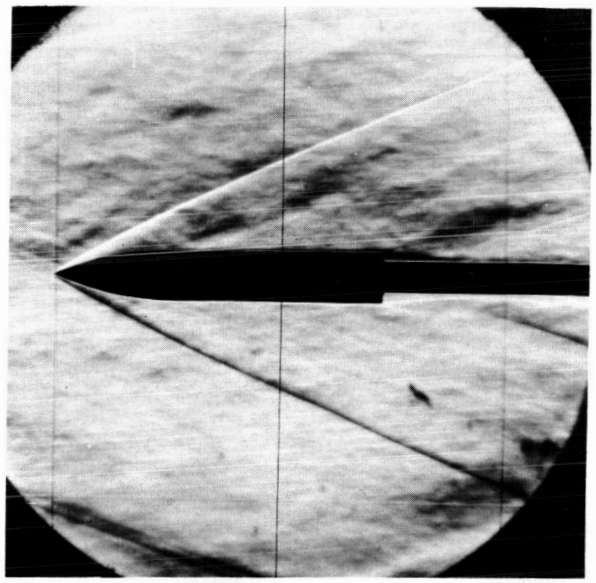

Jet off

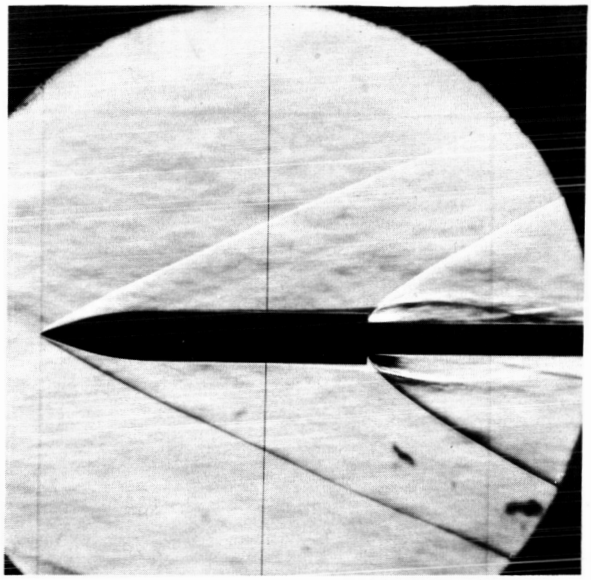

p_j/p_∞=51

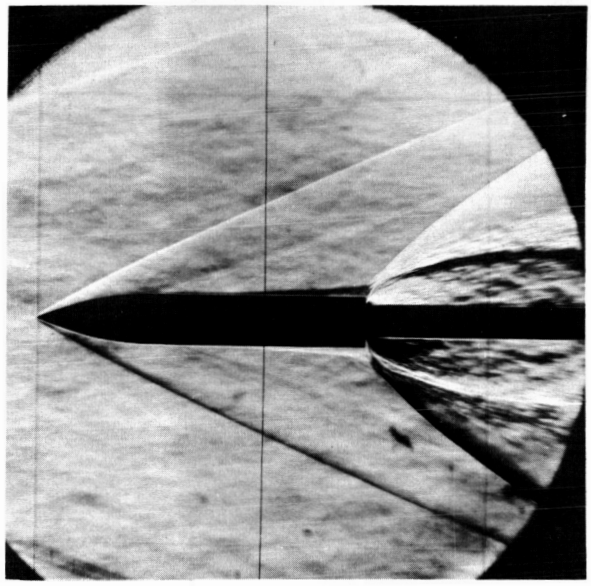

p_j/p_∞=208

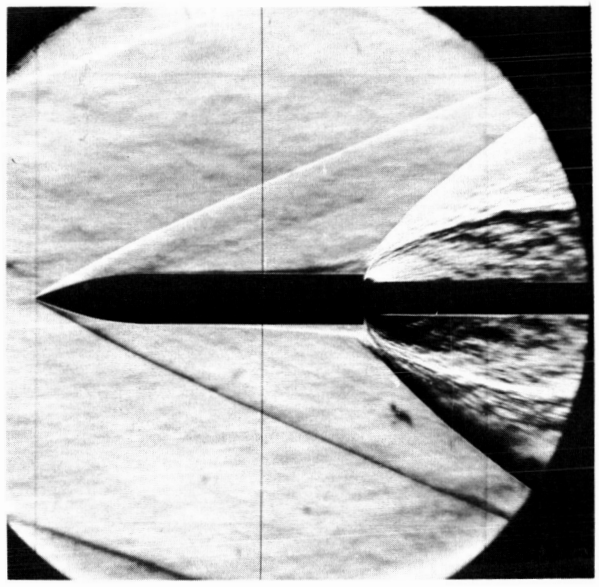

p_j/p_∞=311

(a) $M_\infty = 3.00$; $\alpha = 0^0$. L-70-1649

Figure 9.- Schlieren photographs for configuration 3.

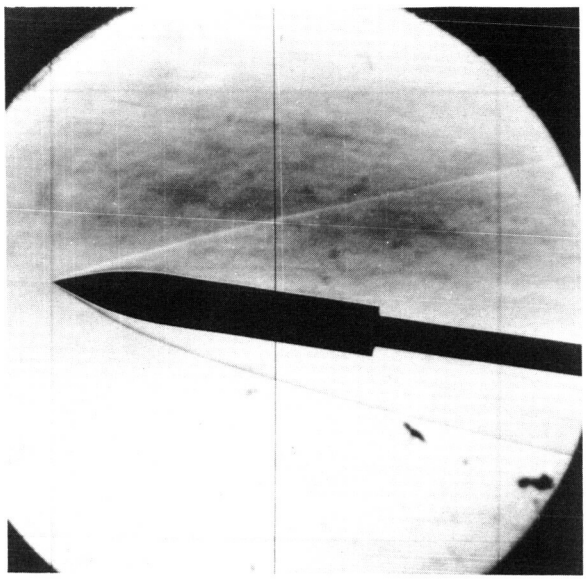

Jet off

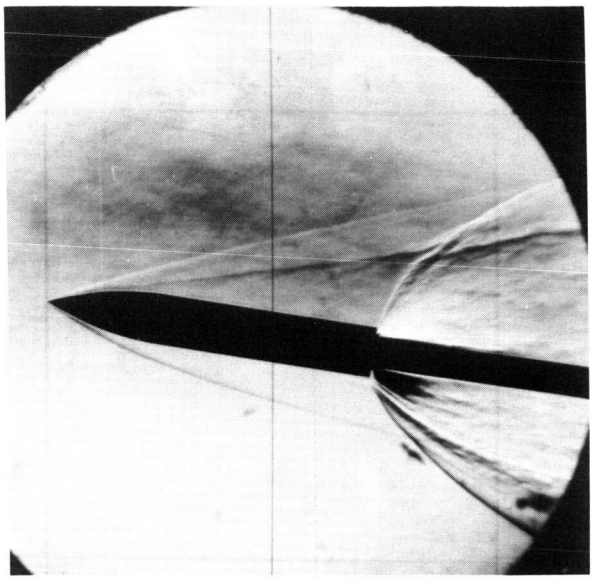

p_j/p_∞=1610

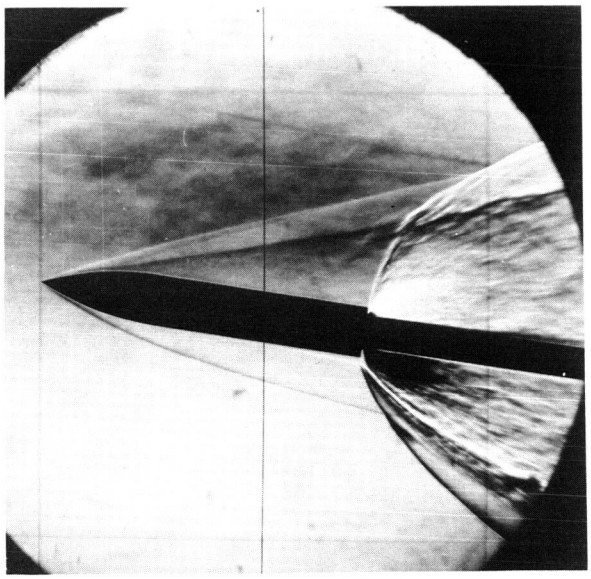

p_j/p_∞=3212

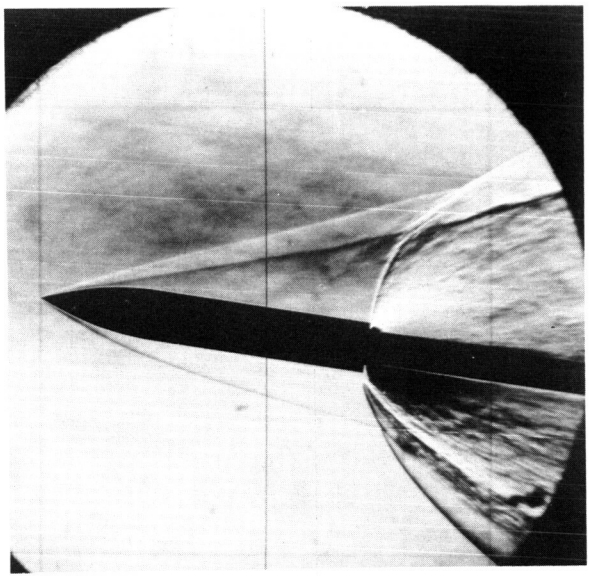

p_j/p_∞=4693

(b) $M_\infty = 6.00$; $\alpha = 8^\circ$. L-70-1650

Figure 9.- Concluded.

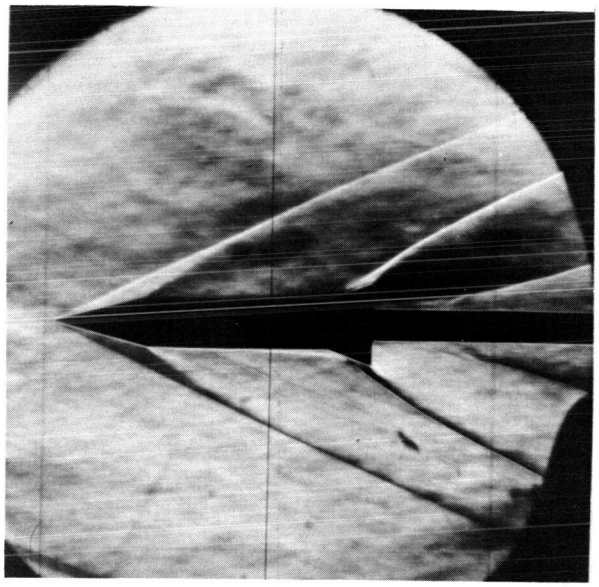

Jet off

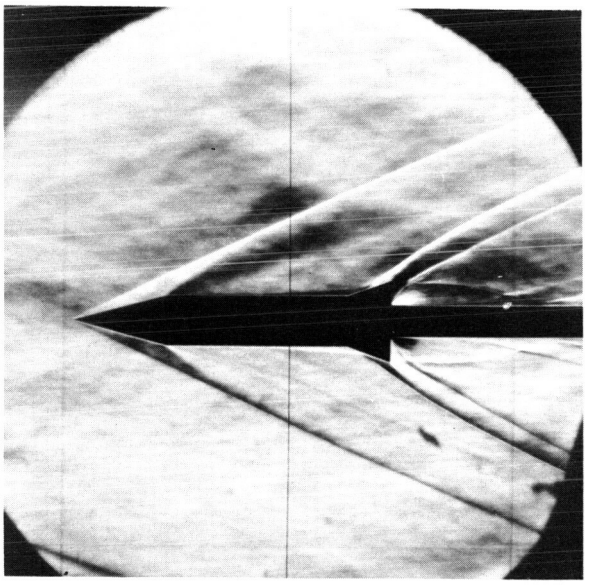

p_j/p_∞=28

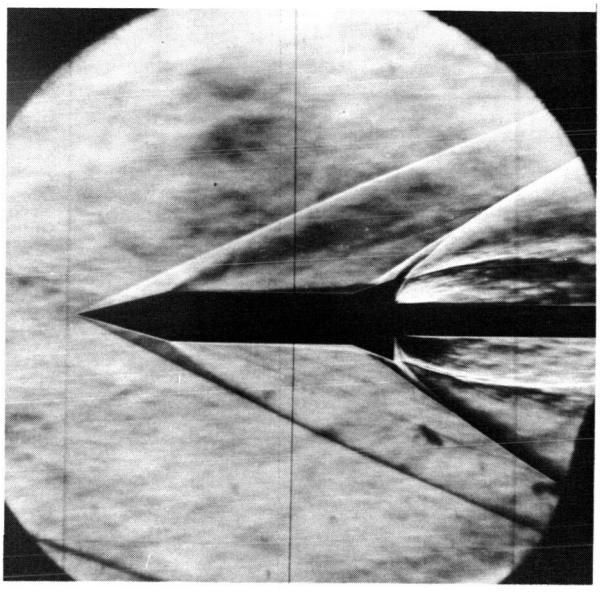

p_j/p_∞=114

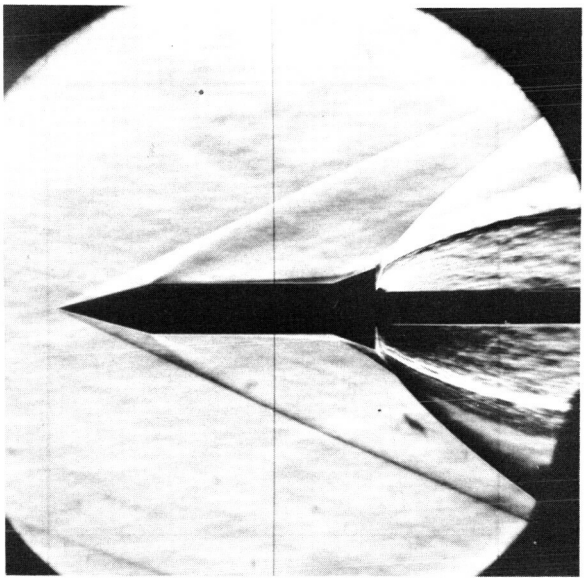

p_j/p_∞=330

(a) $M_\infty = 3.00$; $\alpha = 0^0$. L-70-1651

Figure 10.- Schlieren photographs for configuration 4.

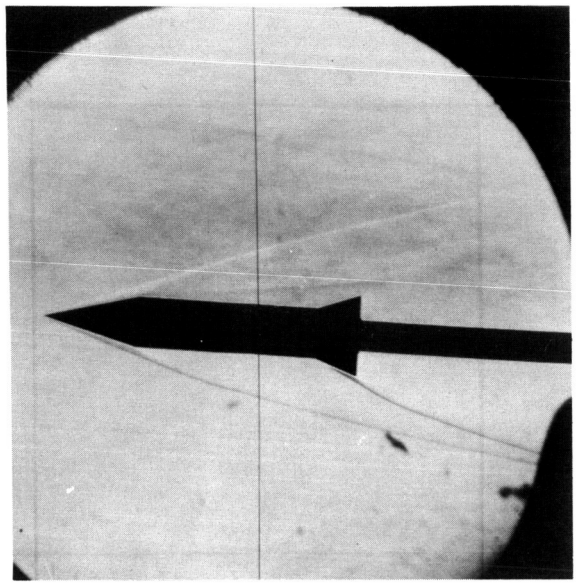

Jet off

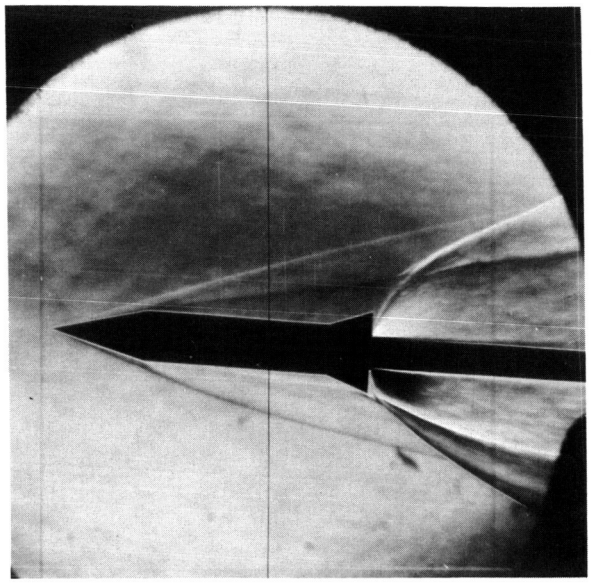

p_j/p_∞=968

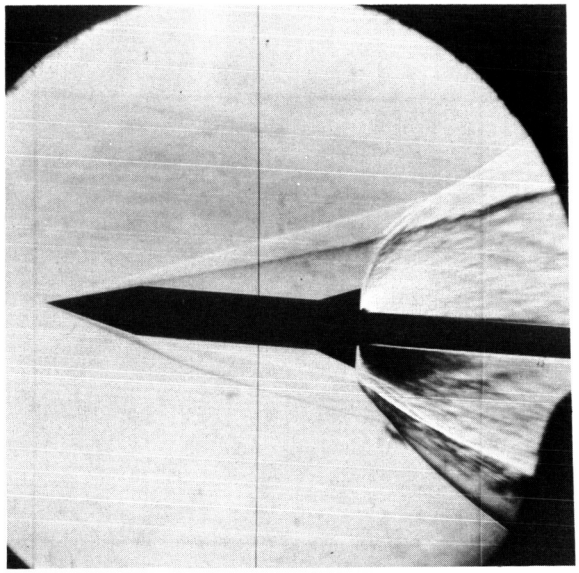

p_j/p_∞=3140

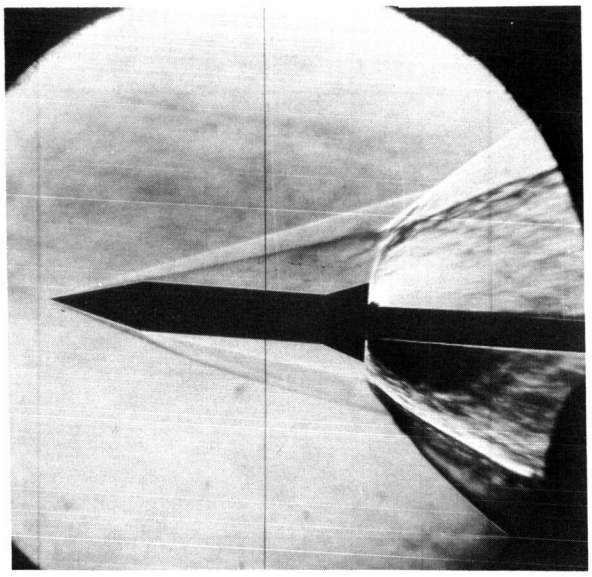

p_j/p_∞=4594

(b) $M_\infty = 6.00$; $\alpha = 4^0$. L-70-1652

Figure 10.- Continued.

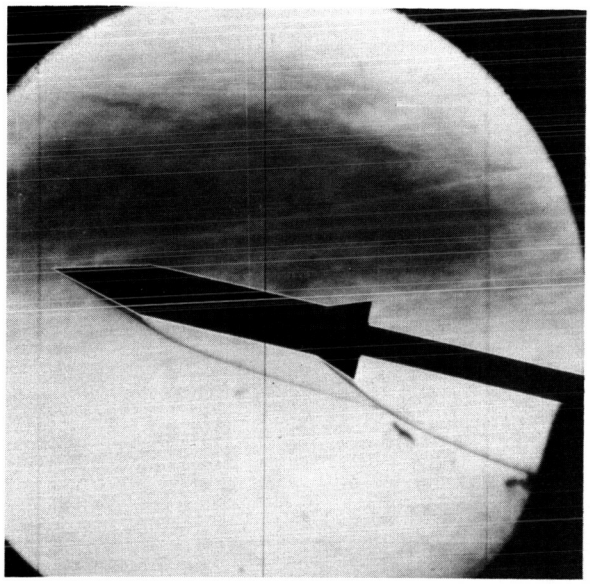

Jet off

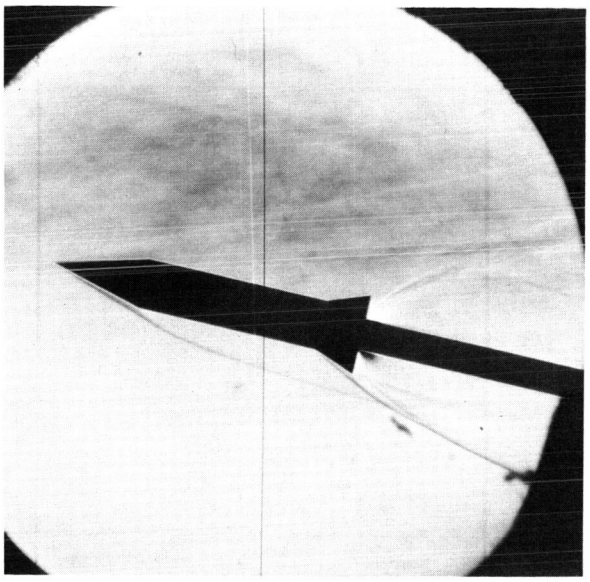

p_j/p_∞=237

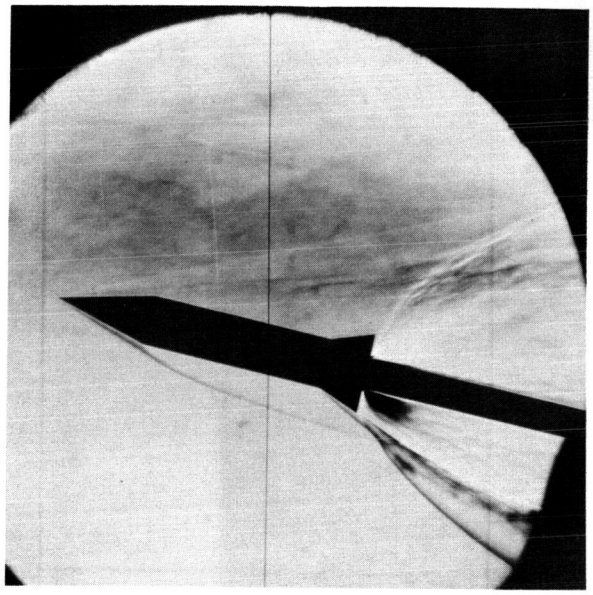

p_j/p_∞=1471

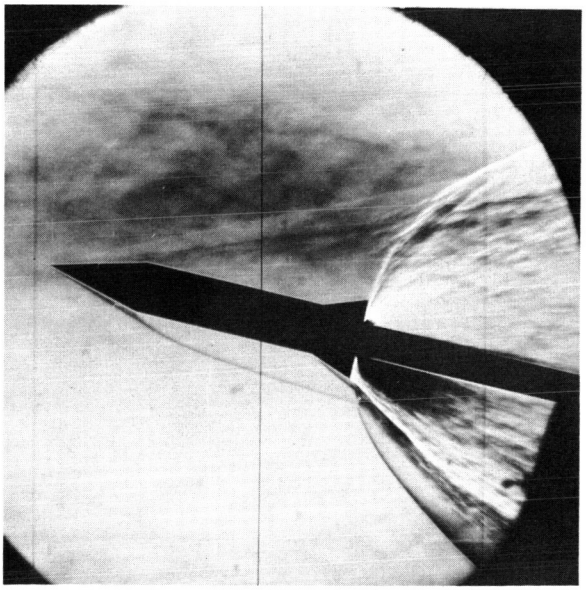

p_j/p_∞=4345

(c) $M_\infty = 6.00$; $\alpha = 13^0$. L-70-1653

Figure 10.- Concluded.

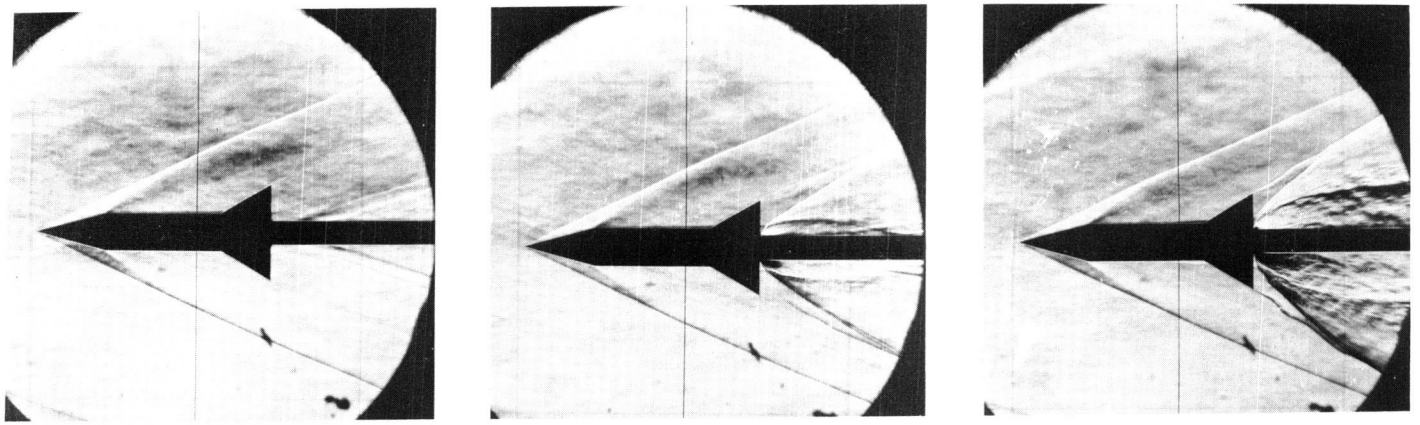

(a) $M_\infty = 3.00$; $\alpha = 0^0$.

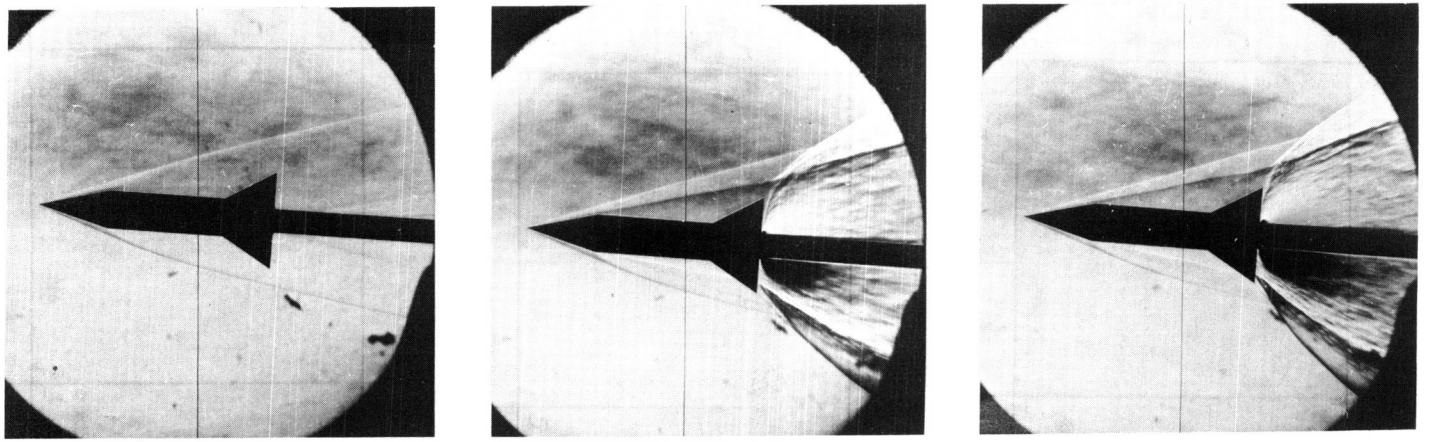

(b) $M_\infty = 6.00$; $\alpha = 4^0$.

Figure 11.- Schlieren photographs for configuration 5.

L-70-1654

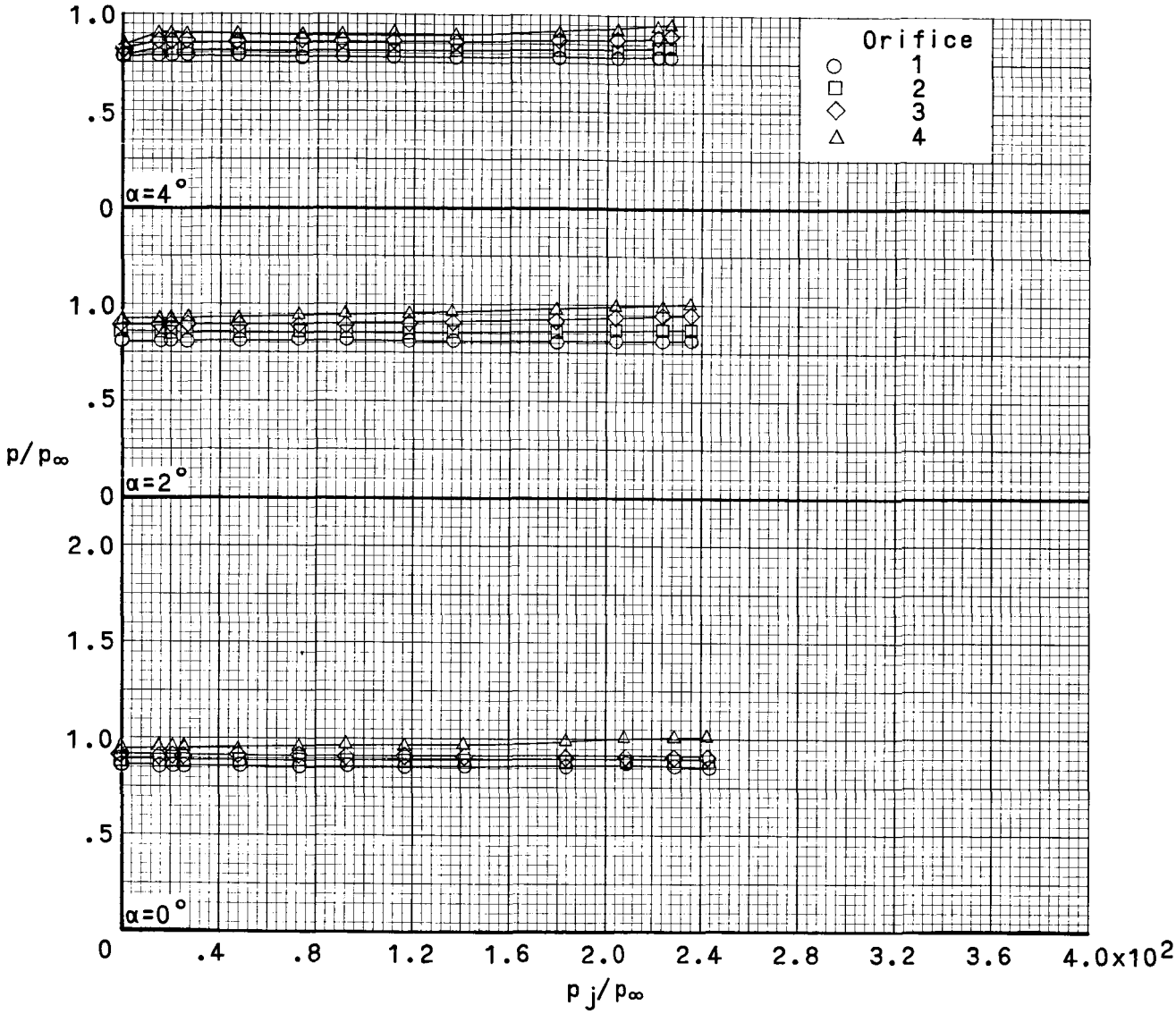

(a) $M_\infty = 3.00$.

Figure 12.- Variation of p/p_∞ with p_j/p_∞ and α for configuration 1.

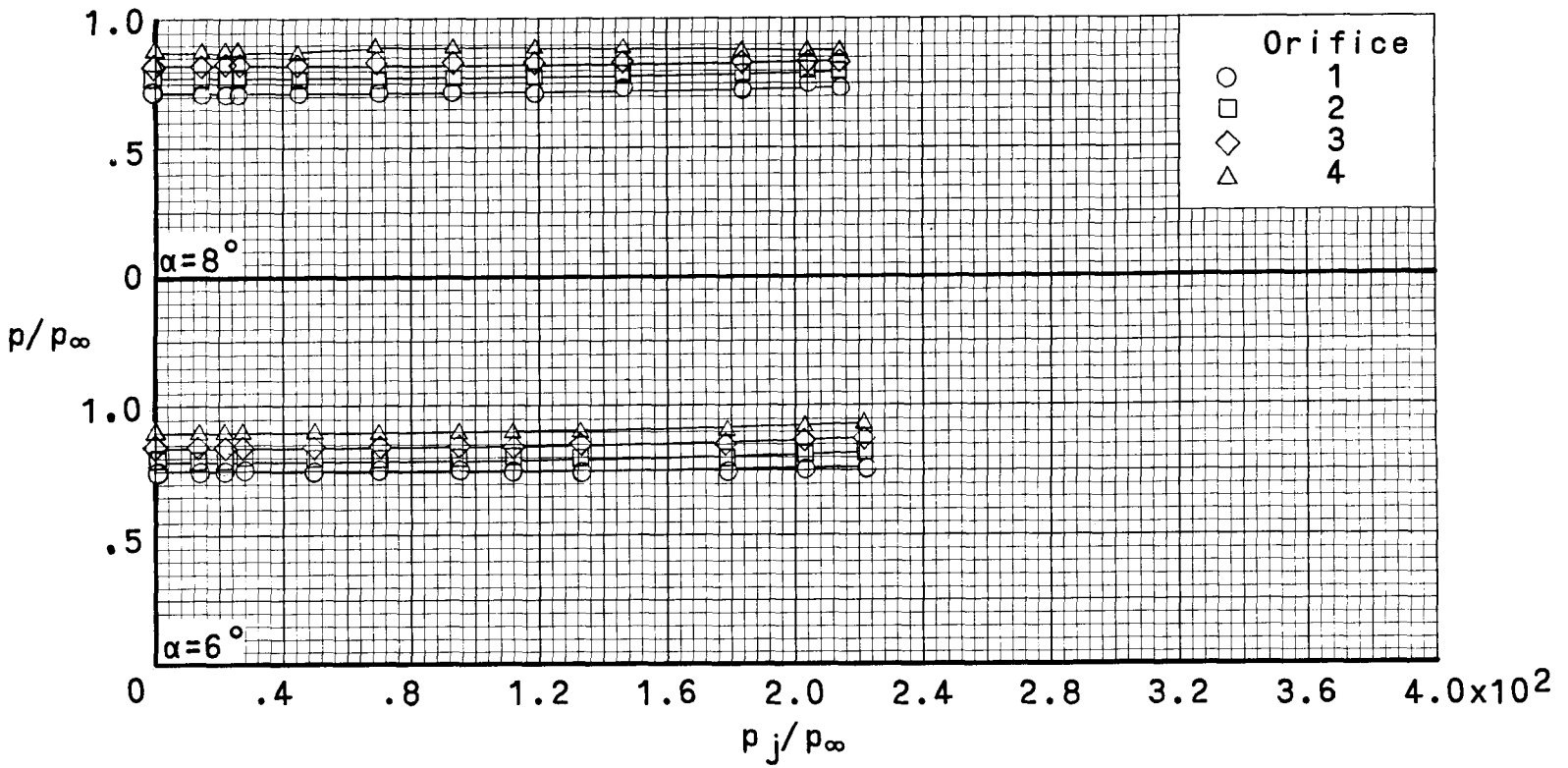

(a) Concluded.

Figure 12.- Continued.

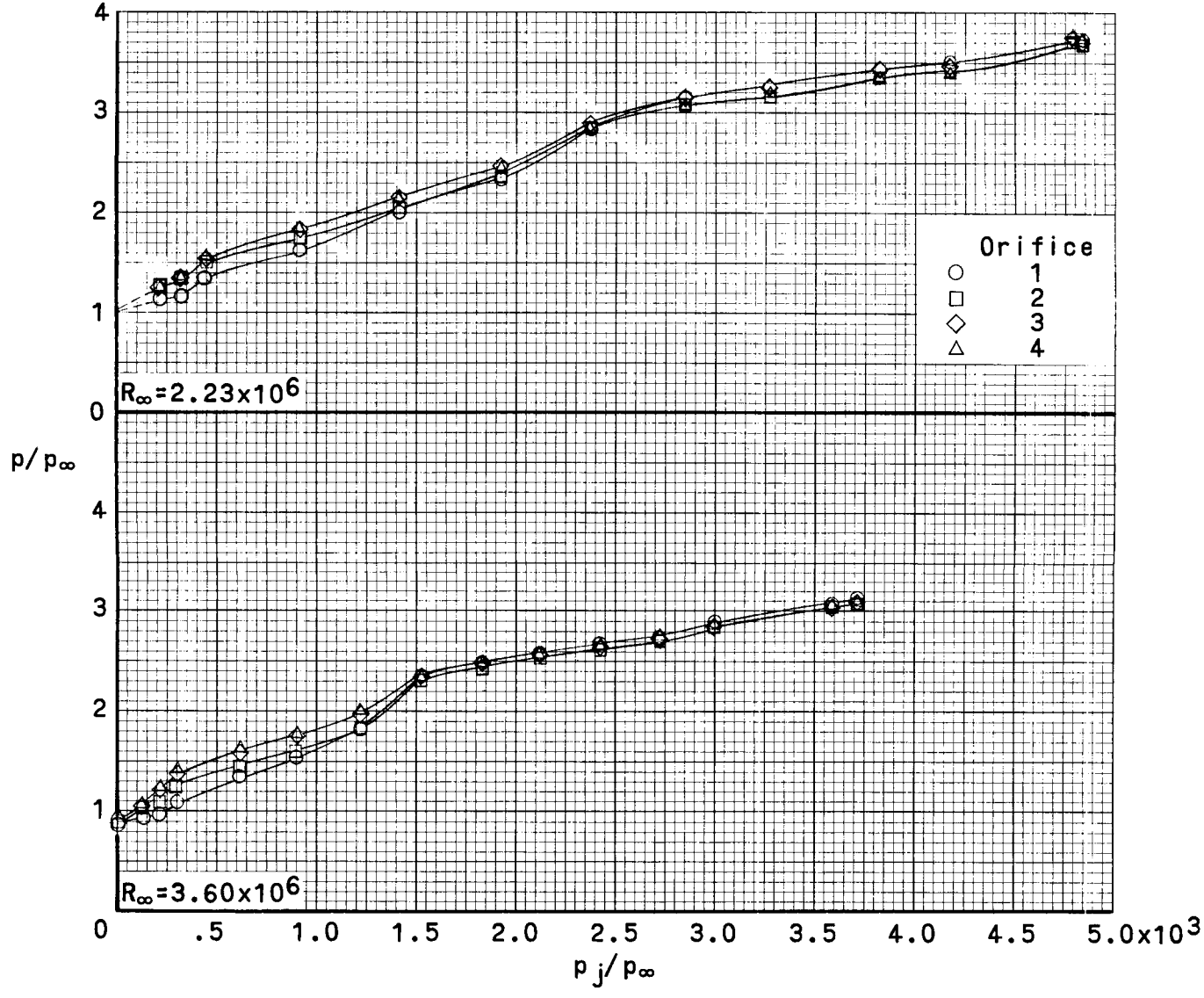

(b) $M_\infty = 6.00$; $\alpha = 0^0$.

Figure 12.- Continued.

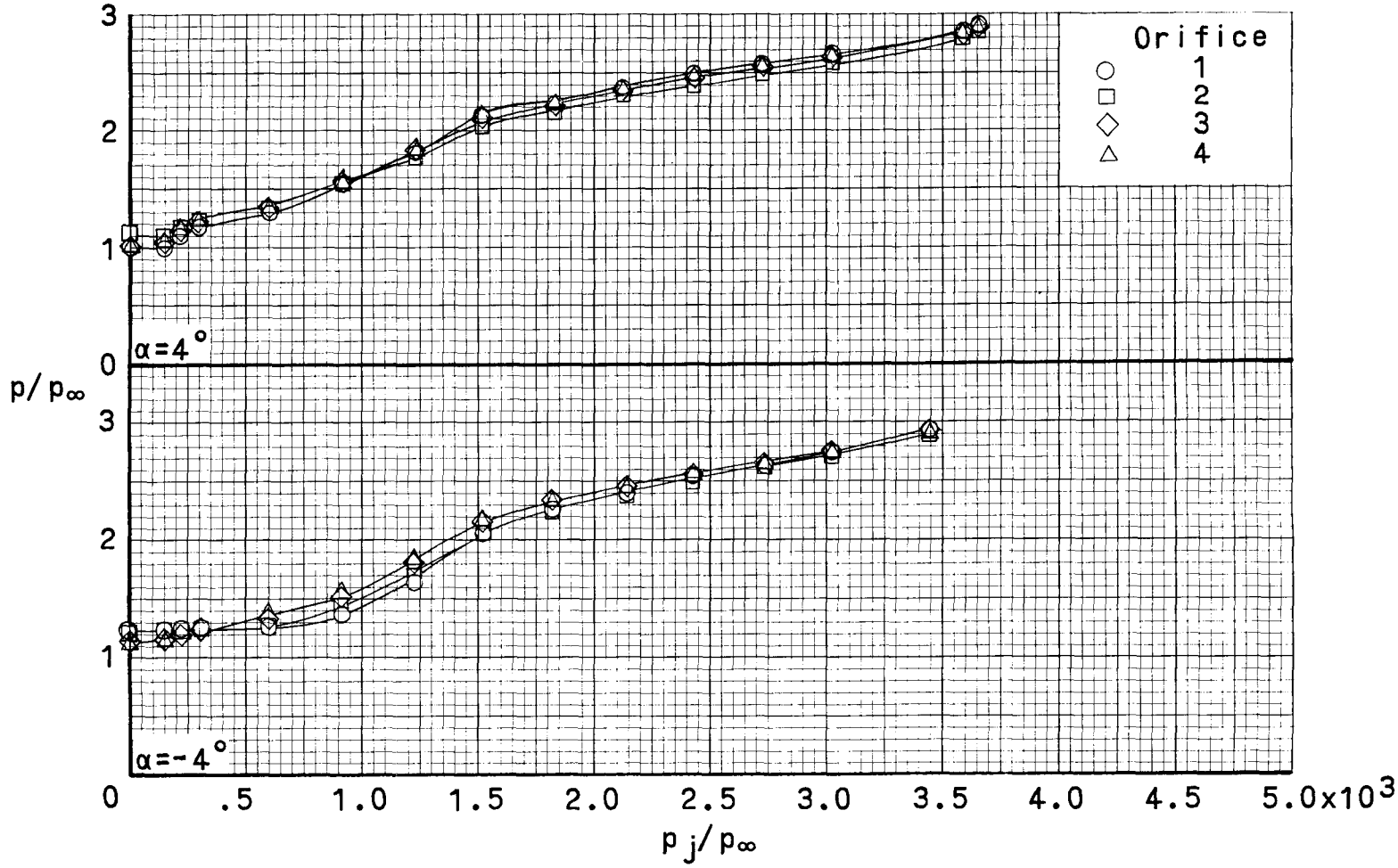

(c) $M_\infty = 6.00$.

Figure 12.- Continued.

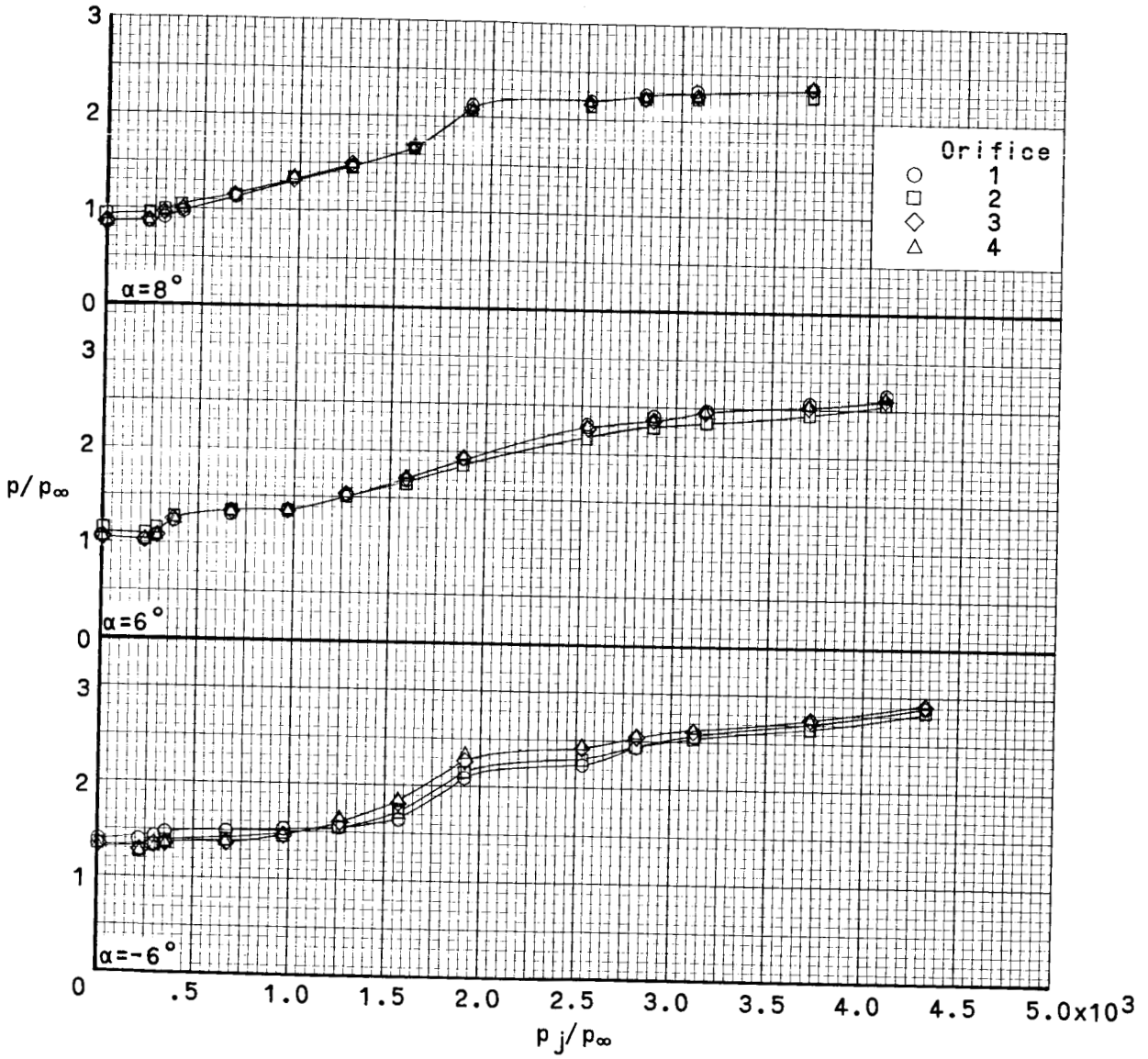

(c) Concluded.

Figure 12.- Concluded.

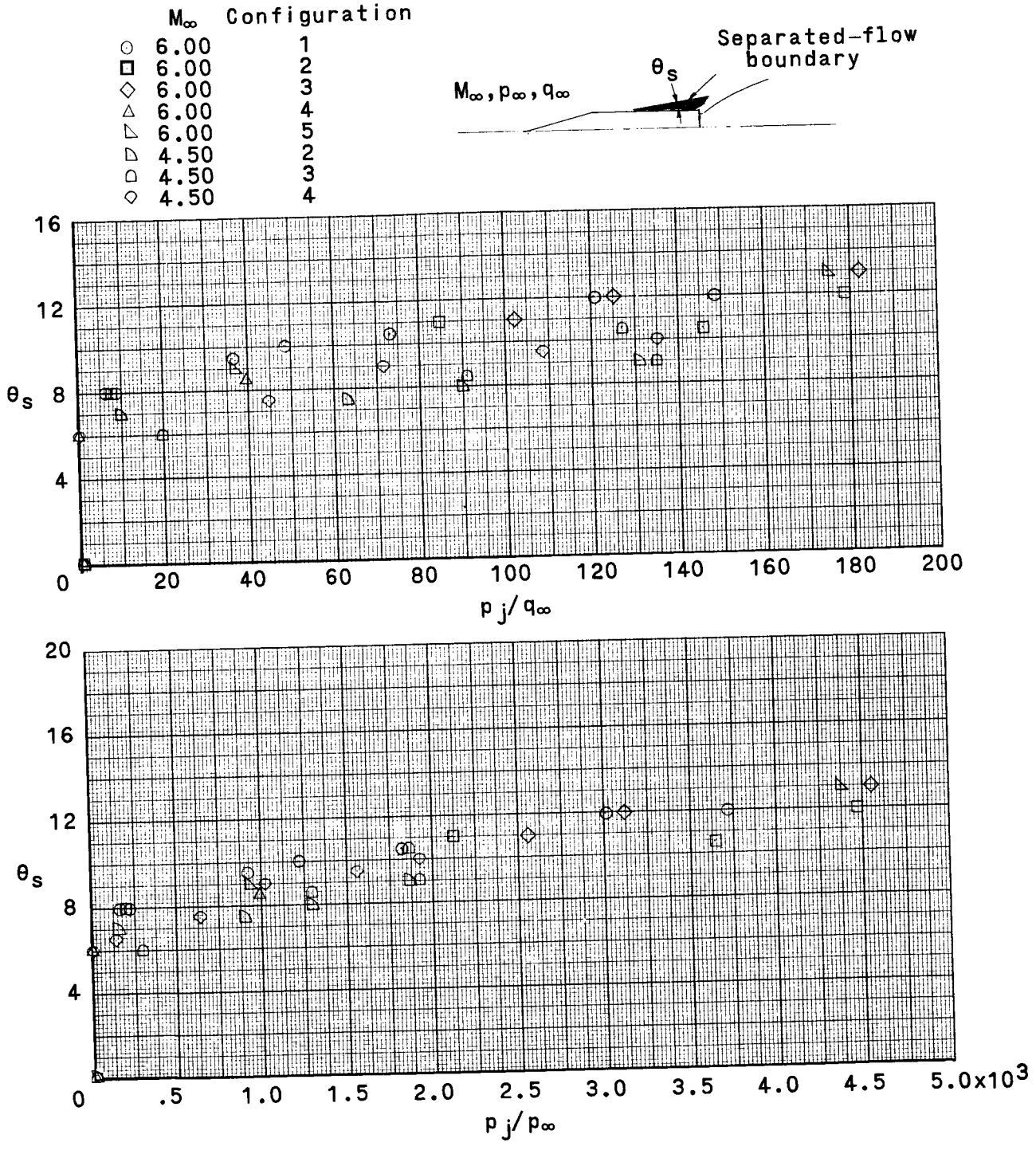

Figure 13.- Variation of θ_s with p_j/q_∞ and p_j/p_∞. $\alpha = 0^0$.

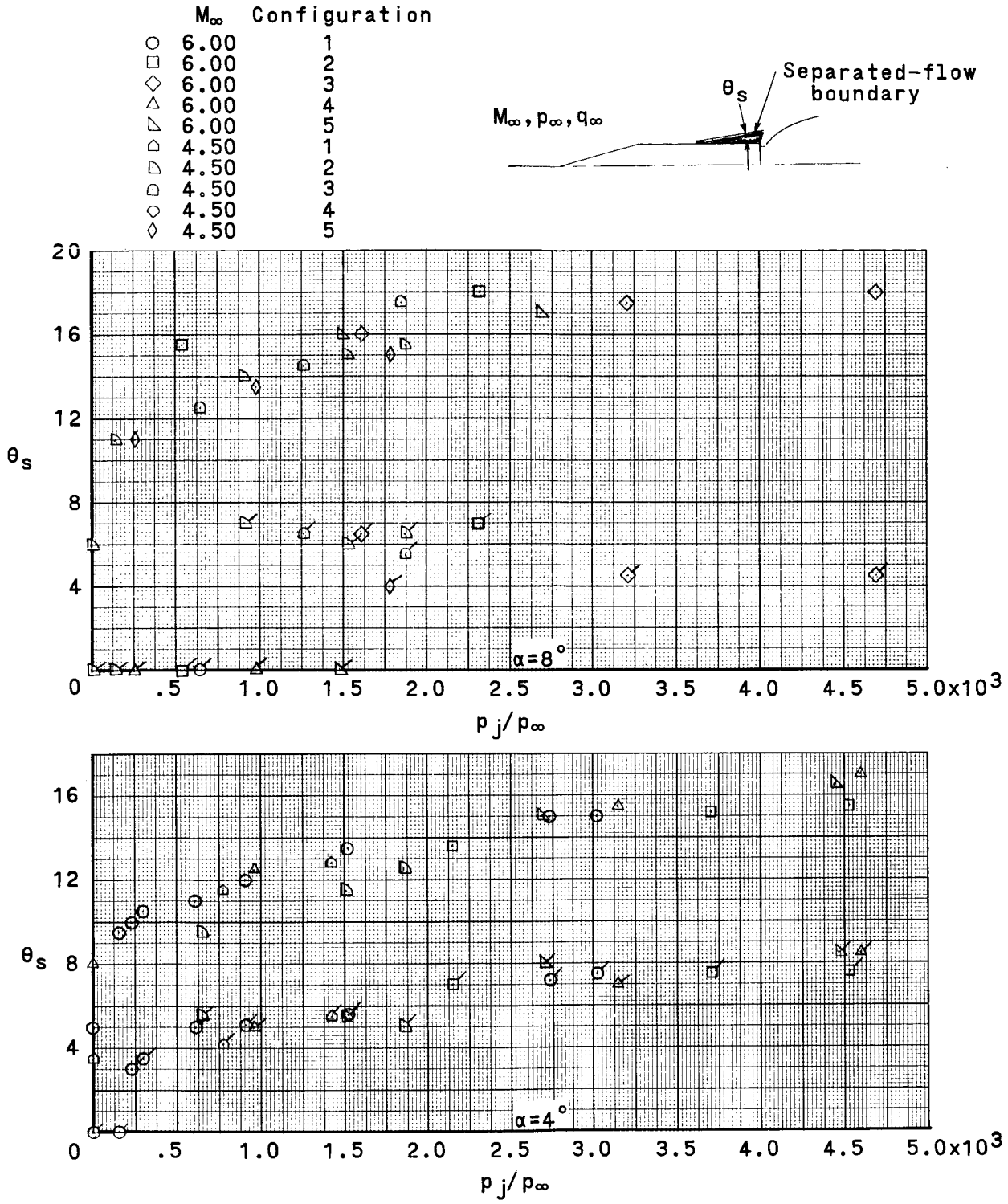

Figure 14.- Variation of θ_s with p_j/p_∞ for angles of attack of 4^0 and 8^0. (Plain symbols represent leeward side; flagged symbols, windward side.)

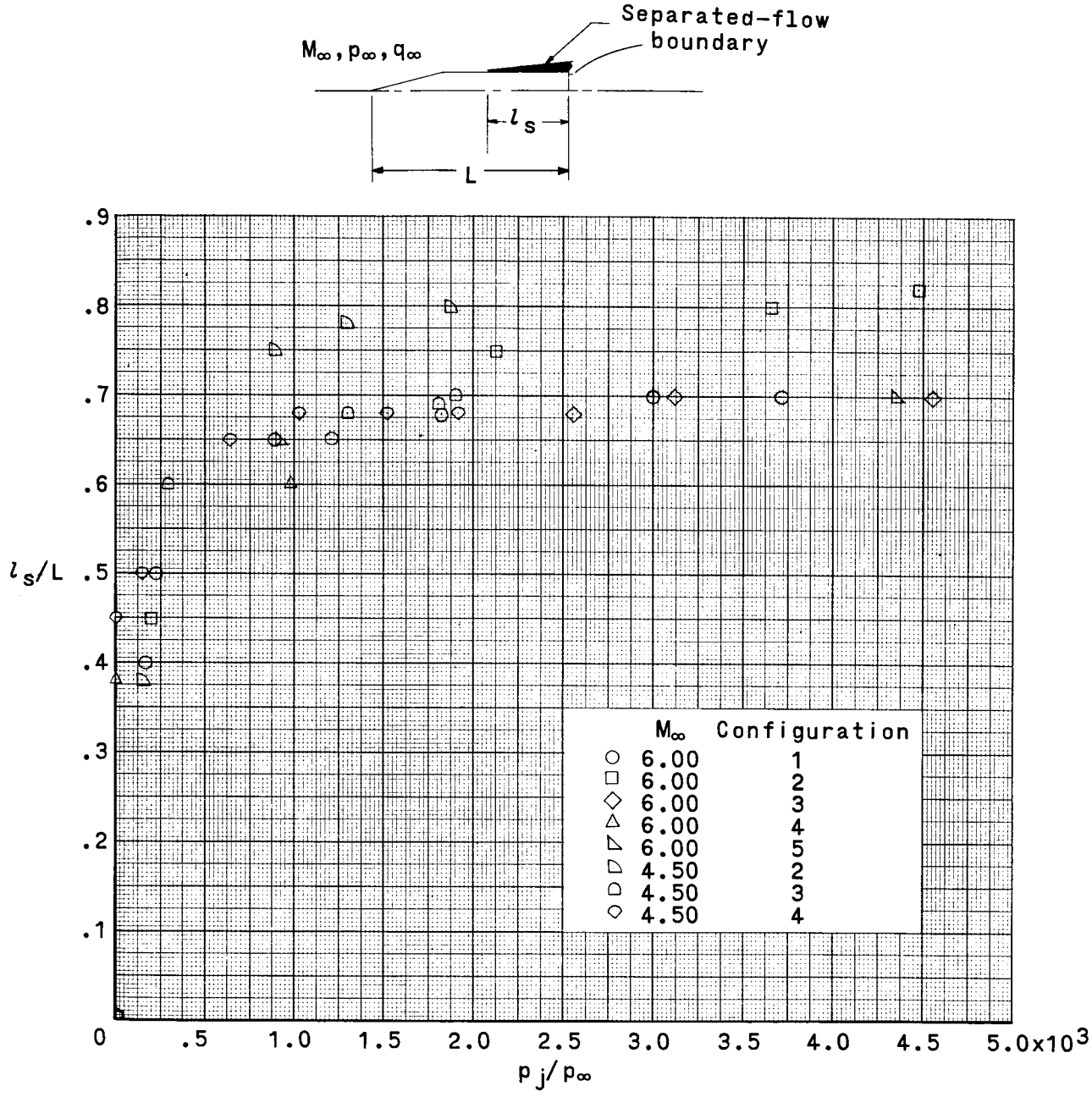

(a) $\alpha = 0^0$.

Figure 15.- Variation of l_s/L with p_j/p_∞.

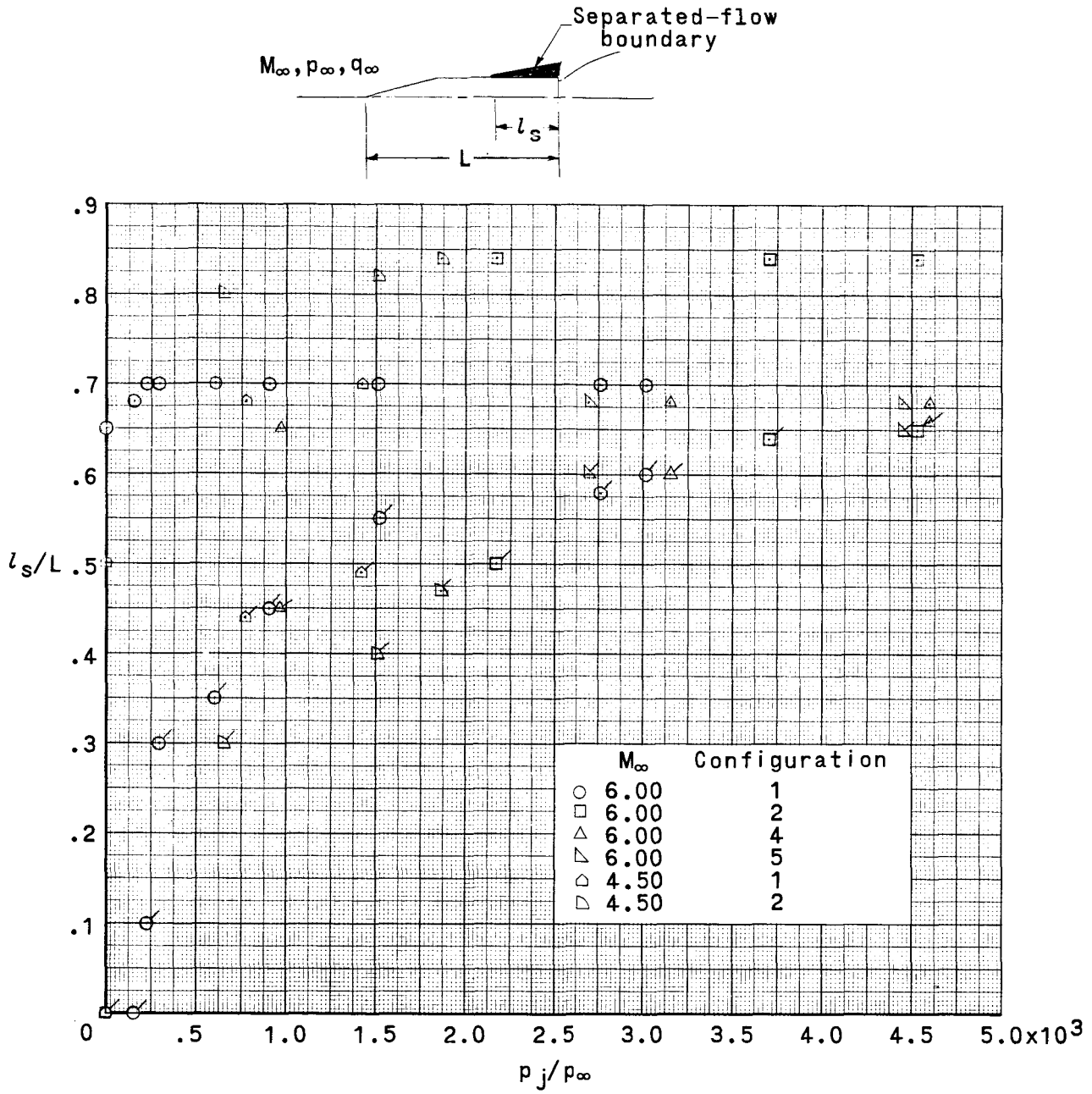

(b) $\alpha = 4^0$. (Plain symbols represent leeward side; flagged symbols, windward side.)

Figure 15.- Continued.

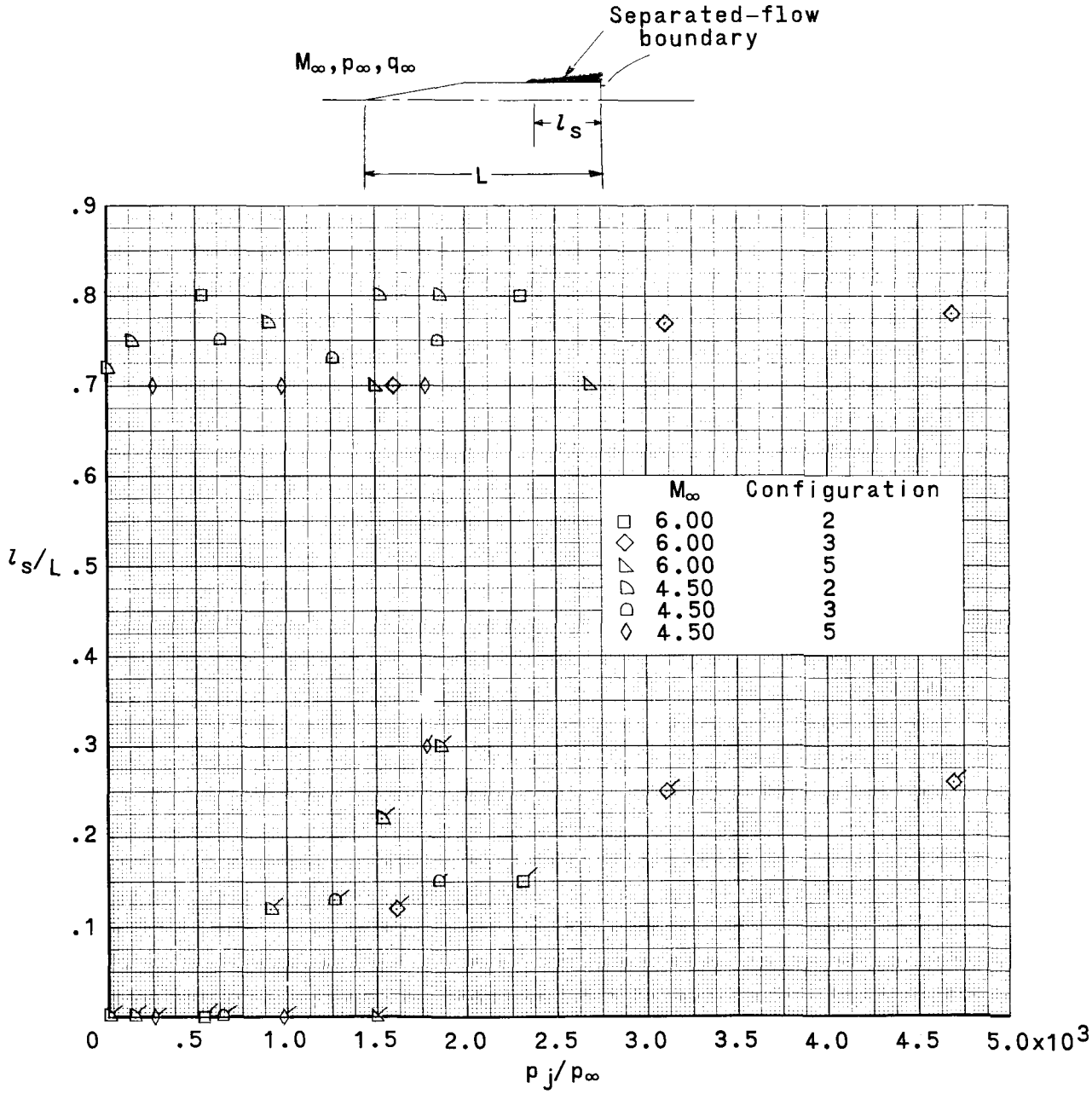

(c) $\alpha = 8^0$. (Plain symbols represent leeward side; flagged symbols, windward side.)

Figure 15.- Concluded.

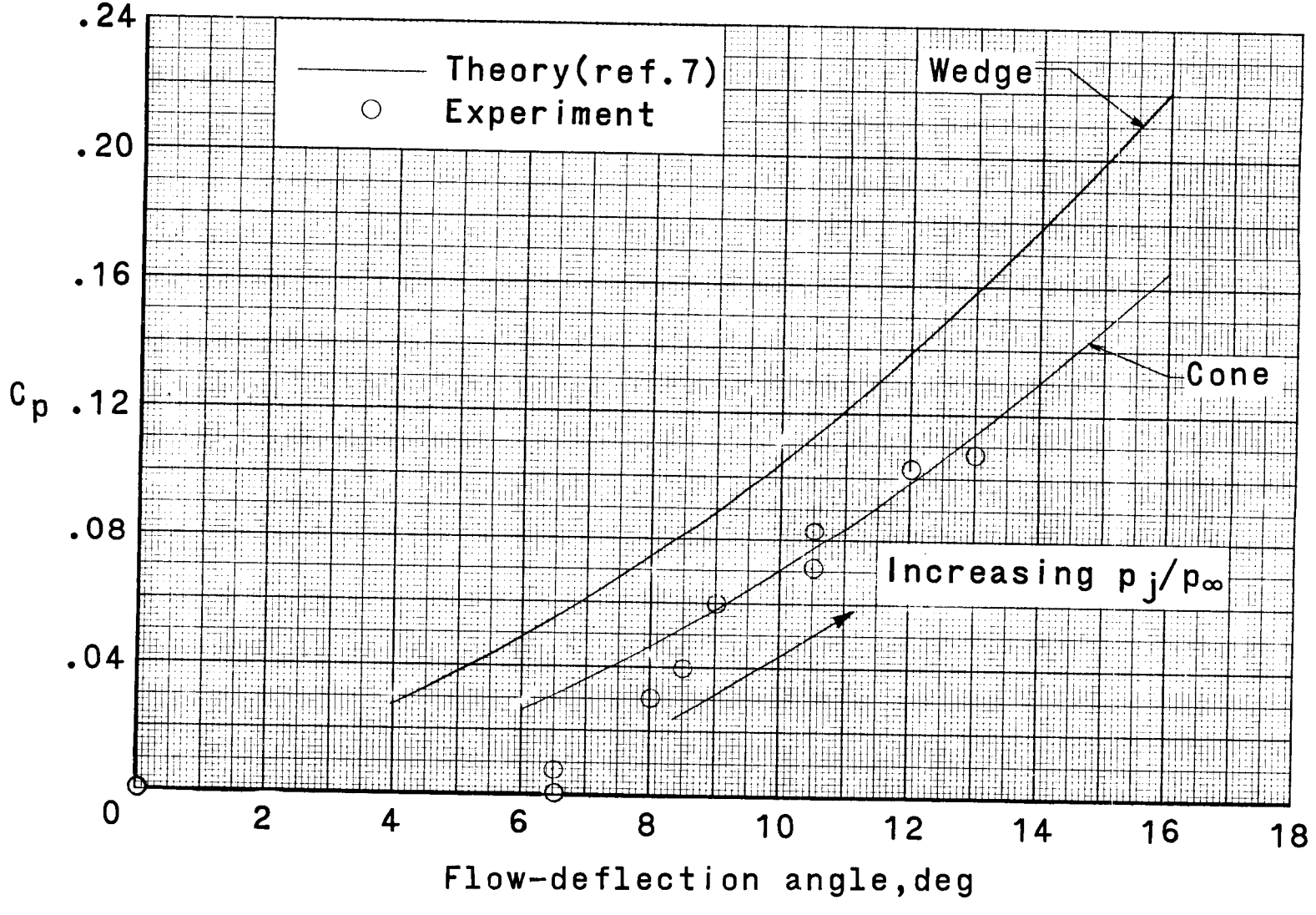

Figure 16.- Variation of C_p with flow-deflection angle for configuration 1. $M_\infty = 6.00$; $\alpha = 0^0$.